Stabilisation of an Entanglement Source

Year in Europe Project

Michael Brownnutt

June 2002

Universität Erlangen–Nürnberg
Physikalisches Institut
Lehrstuhl für Optik
Prof. Dr. G. Leuchs

Summary

Much new science, and many novel applications, are opened up by the possibility of having so called entangled quantum states. These states exhibit specific non-local correlations that are not possible classically. The Quantum Information Processing group (QIV) at Erlangen University, Germany, carries out experiments into the possible uses of these states in the field of quantum optical communication. To do this an entanglement source is required that consistently produces states with a high degree of entanglement. Using the experimental train shown in figure 1 the group had achieved entanglement using bright beams. Two quantum noise reduced, or squeezed, beams are produced with a Non-linear Optical Loop Mirror (NOLM). These are entangled by being interfered on a 50:50 beam splitter.

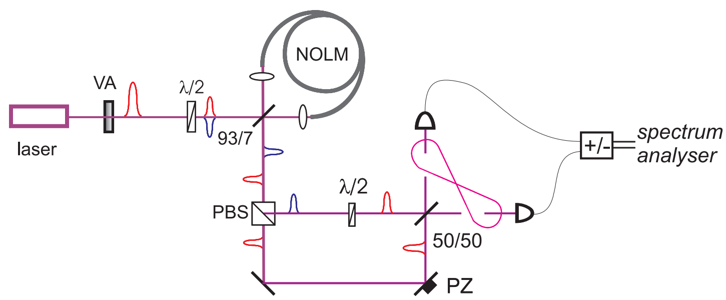

Figure 1: Experimental train. The laser power is set by a variable attenuator (VA). By setting the polarisation using a half-wave plate (λ/2), two orthogonally polarised squeezed beams are produced by the Non-linear Optical Loop Mirror (NOLM). The squeezed pulses separated at a Polarisation Beam splitter, and interfered on a 50:50 beam splitter. This produces entanglement of bright beams.

While entanglement had been achieved, the quality of entanglement was limited, and the ease of experimenting hindered, by several sources of instability in the setup. In particular the drift in laser power reduced the degree of squeezing achieved, and the drift in interference phase at the interferometer reduced the possible degree of entanglement. The first aim of this project was to stabilise the power output of the laser using a half-wave plate and polariser to attenuate the beam. These were controlled via a PC, and monitored via a DC detector. This was required so that the degree of squeezing achieved by the NOLM could be held near the optimal value.

The scheme was implemented using components already employed by the group, and so with minimal disturbance to the present setup, or outlay on new materials. Once implemented, the system could realise regulation of $\pm$ 0.75%. This is sufficient control to keep the degree of squeezing to within 0.5dB of the maximum value.

The detector developed for the task was characterised, and can now also be used as a general purpose DC detector to, for example, monitor the beams for phase regulation. A motor control program which was written can be used in other experiments where the laser power must be set, regulated or altered. It is already being used to control the laser power for experiments investigating squeezing in mocrostructured fibres and squeezing as a means of amplifier noise reduction.

Once constant squeezing was achieved, the second aim of the project was to control the interference phase at the beam splitter, ideally to an accuracy of better than 1%. This was required so that the optimum degree of entanglement of the two squeezed beams could be achieved, and held. In the case of the ideal interference phase, the entangled beams are equally bright. Phase stabilisation was achieved by an electronic feedback system which measures the beams' brightness and accordingly alters the arm lengths of the interferometer via a piezo-electric controller. The feedback ensured that the output beams were of equal brightness, and hence, optimally entangled.

Several controller designs were evaluated for the feedback system, and a Proportional-Integral (PI) controller was chosen. A difference amplifier and PI-controller were designed to remove the measured drift, then built and tested. The regulation system had a systematic error of 1.9% and a statistical error of 0.02%.

As well as being used in the train shown above, the phase control system will be used to control the interference phase for an entanglement swapping experiment.

Zusammenfassung

Viele neuartige Anwendungen in der Physik ergeben sich durch die Verwendung von sogenannten ,,verschränkten Quantenzuständen”. Diese Zustände weisen bestimmte nichtlokale Korrelationen auf, die klassisch nicht möglich sind. Die Quanteninformationsverarbeitungsgruppe (QIV) in Erlangen, Deutschland, führt Experimente durch, die mögliche Verwendungen dieser Zustände im Bereich der quantenoptischen Kommunikation erforschen. Herfür ist eine Verschränkungsquelle notwendig, die hochgradig verschränkte Zustände zuverlässig erzeugen kann. Mit dem Aufbau, der in Bild 1 dargestellt ist, hat die Gruppe Verschränkung mit hellen Strahlen erzielt. Zwei quantenrauschberuhigte, oder gequetschte, Lichtstrahlen werden durch Verwendung eines nichtlinearen, optischen Schlaufespiegels (NOLM) erzeugt. Diese werden durch Überlagerung an einem 50:50 Strahlteiler verschränkt.

Obwohl Verschränkung erreicht wurde, war die Qualität der Verschränkung begrenzt, sowie die Handhabbarkeit durch einige Instabilitätsquellen eingeschränkt. Vor allem, driftete die Laserleistung, wodurch der Quetschgrad reduziert war. Die Drift der Interferenzphase am Strahlteiler reduziert den maximal erreichbaren Verschränkungsgrad. Das erste Ziel dieses Projekts war die Stabilisierung der Laserleistung. Das war notwendig, um den Quetschgrad in der Nähe des optimalen Wertes zu halten. Unter Verwendung einer Halbwellenplatte und eines Polarisationsstrahlteilers, wurde der Strahlgezielt abgeswächt. Der Winkel der Halbwellenplatte wurde über einen PC eingestellt, die Laserleistung mit einem DC Detector gemessen.

Das Schema wurde mit Komponenten aufgebaut, die in der Gruppe schon verwendet werden damit es sich mit minimalem Aufwend in den bestehenden Aufbau einfügen lässt. Mit diesem Aufbau konnte die Laserleisung auf $\pm$ 0.75% genau geregelt werden. Dies ist ausreichend um den Quetschgrad innerhalb von 0.5dB des Maximalwert es festzuhalten.

Der Detektor, der für diese Aufgabe entwickelt wurde, wurde charakterisiert, und kann als Mehrzweckdetektor benutzt werden, z.B. um die Strahlen für Phasenstabilisierung zu überwachen. Ein Motorsteuerprogramm, das geschrieben wurde, kann für andere Experimente benutzt werden, in welchen die Laserleistung gesteuert, geregelt, oder verändert werden muß. Er wurde schon in Experimenten benutzt, die gequetschtes Licht in mikrostrukturierten Fasern erzeugen und Möglichkeiten der Rauschreduktion von Verstärkerrauschen untersuchen.

Das zweite Ziel des Projekts war, die Interferenzphase am Strahlteiler zu regeln, idealeweise mit einer Geauigkeit von mehr als 1%. Dies ist notwendig um den optimalen Wert der Verschränkung der zwei Strahlen zu erreichen, und stabil zu halten. Die Aufgabe wurde durch ein elektronisches Rückkopplungssystem gelöst. Hierfür wird die Strahlhelligkeit gemessen, und entsprechend die optische Wegänge, durch einen Piezo-elektrischen Regler

geändert. Die Rückkopplung stellte sicher, daßdie Ausgangstrahlen gleich hell waren, und damit maximal verschränkt waren.

Einige Regler wurden für das Rückkopplungsschema bewertet, und schließlich ein Proprtional-Integral (PI) Regler ausgewählt. Ein Differenzverstärker und ein PI-Regler wurden entworfen, gebaut und getestet, um die gemessenen Phasendrifts zu beseitigen.

Das Regelsystem hatte einen systematischen Fehler von 1,9% und einen statistischen Fehler von 0.02%. Der Regler kann nicht nur für die Phasenstabilisierung für der Verschränkunsquelle benutzt wurden, sondern wird auch die Interferenzphase eines Verschränkungsaustauschexperiments stabilisieren.

Contents

Chapter 1

Introduction

Quantum information processing opens up many new areas of information processing that are simply not possible using classical methods. For example, Shor devised a quantum algorithm that could factorise large numbers efficiently [1]. All that is now required is a quantum computer that can implement the algorithm, and what are currently the world's securest codes could be cracked in seconds [2]. At the same time, quantum mechanisms can provide new cryptographic communication systems that are literally uncrackable [3]. Such systems have been demonstrated that can work even over extended distances, though these are still in their infancy and have low bit rates (recently reported: 4 kBit/s over 10km [4], compared to 10^{12} bit/s for classical long haul fibre optic communication.) Therefore, 18 years after the first protocol for quantum coding was suggested, work still continues on a practical experimental realisation. One of the problems for quantum information processing is the difficulty of generating, preparing and handling single photons or atoms [5].

The Quantum Information Processing group (QIV) at Erlangen University uses instead squeezed solitons. These non-classical, bright (10^9 photon) pulses can be used as macroscopic quantum objects for both purely quantum, and quantum-assisted classical communication [6], and potentially have applications for quantum computing [7]. They have the advantage over single photons that there are readily available, reliable sources of pulsed, coherent light (notably lasers) and efficient detectors. Sources of individual photons on demand, however, are still under development [8]. Solitons have the further advantage that they can be transmitted with low losses at high bit rates using standard telecommunications optical fibre. [1]

Given this motivation, this chapter discusses squeezing, and the main purpose for which it is used at Erlangen: entanglement. Below, the nature and a method of experimental realisation of each phenomenon is explained. Two significant sources of experimental difficulties are presented, and the aims of this project are outlined in light of these difficulties.

[1] Solitons are standardly modulated at 2.5 GBit/s. In principle this could be used for quantum communication data rate of order 10 MBit/s, although this has never yet been implemented. [9]

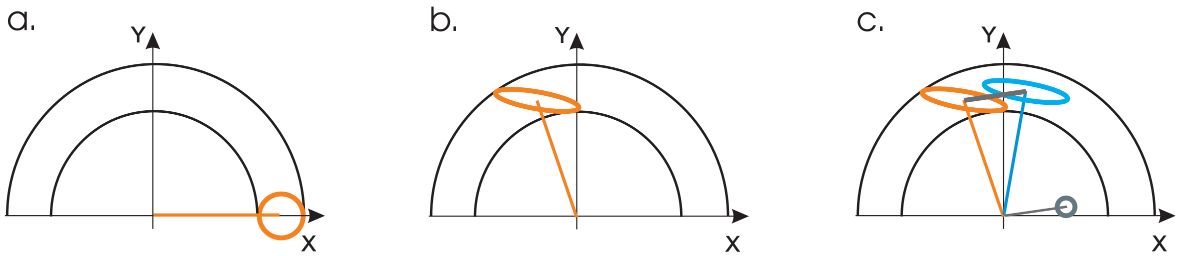

Figure 1.1: (a) Shows a coherent state as emitted by a laser. The grey circle represents the uncertainty in the amplitude (radial direction) and phase (azimuthal direction). After traveling some distance through a non-linear medium, the uncertainty region has undergone an intensity-dependent phase shift (b). If, on leaving the medium, the state is interfered with a weak pulse of the correct amplitude and phase, its uncertainty is reoriented so that the squeezing can be observed in direct detection (c) [15].

1.1 Squeezed light

In a coherent state of light, as emitted by a laser, the photon number follows Poisson statistics. For a Poisson distribution the variance is equal to the mean. This gives a quantum uncertainty in the amplitude of the pulse. Amplitude-squeezed light is in a state where the uncertainty in the amplitude is less than that of the coherent state [10]. The uncertainty principle is not violated as the uncertainty in the conjugate phase variable increases.

Such light is useful in otherwise purely classical situations, for example, in repeaters for telecommunications. If the light is amplitude squeezed immediately after amplification, the inter-symbol interference over the following fibre stretch, and thereby the bit error rate, can be reduced [10]. Of more direct interest in the context of the current project is that squeezed beams can be used for producing entanglement [11]. The exact nature of entanglement is covered in more detail in section 1.2. Bright-beam entanglement can be achieved by various means. Coherent, ie unsqueezed, light can be entangled using nonlinear interactions [12]. Alternatively, if the individual pulses are exposed to a non-linear effect, and thereby squeezed, entanglement can be achieved by thereafter using only linear interactions [13]. The two different methods lend themselves to different applications, depending on the hardware required. Uses of entanglement involving fibre optics and telecommunications wavelengths are well served by the second method.

When light travels through a medium, it undergoes a phase shift related to the index of the medium. In linear media, the index, and so the phase shift, is independent of the intensity of the light. Some non-linear media, however, exhibit a so-called non-linear Kerr effect, whereby the index of the material is given as [14]:

$$n = n_0 + n_2 I \tag{1.1}$$

where: n is the material's refractive index
I is the intensity of the light
n_0 is the linear refractive index

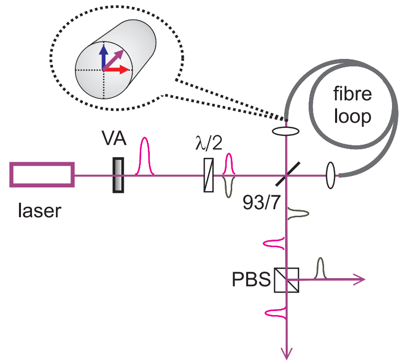

Figure 1.2: Optical train used to provide squeezed bright beams. The laser power can be adjusted using the variable attenuator (VA) so as to set the correct power to realise the required phase shift, as explained in figure 1.1. The half-wave plate ($\lambda/2$) orients the polarisation so that the NOLM produces two orthogonally polarised, squeezed beams. These can be separated at a polarisation beam splitter (PBS). (Adapted from [16])

n_2 is the nonlinear refractive index

Thus high intensity light traveling through such media undergoes a larger phase shift than light of lower intensity, as shown in figure 1.1.

Figure 1.1 shows a phasor diagram, where the X and Y axes are the phase and amplitude quadratures, which correspond to the real and imaginary parts of the field. The amplitude of a field is given by a vector in the radial direction, and the angle from the X axis is the beam's phase. The eliptical regions in the figure are the quantum uncertainties in amplitude and phase. An amplitude measurement will measure uncertainty in the radial direction, which is clearly the same after traveling through the medium as it was before. However, if upon leaving the medium, the light pulse is interfered with a weak beam of the correct amplitude and phase, it is reoriented such that an amplitude measurement will give an uncertainty smaller than that of the coherent state. The degree of squeezing of a state is measured as the uncertainty of the state in deciBels (dB) compared to the uncertainty of the coherent state. The scheme illustrated in figure 1.2 uses this Kerr nonlinearity to amplitude squeeze pulsed laser light in a fibre. By coupling in light with a polarisation at 45^o to the fibre's optical axis, it is possible to get two orthogonally polarised, independently squeezed beams, one on each of the main axes. A fibre used in this way and built into an interferometer as shown is termed a Non-linear Optical Loop Mirror, or NOLM. The asymmetry of the beam splitter means that two beams, one weak and one strong, counter propagate in the fibre. The weak beam is essentially unaffected by the fibre nonlinearity, and provides the reorienting beam shown in figure 1.1c.

The necessary phase relation of the strong and weak beams is only fulfilled at certain optical powers (figure 1.3). To consistently achieve optimal squeezing it is therefore required that the incident power can be set to and maintained at the required value. Due to effects caused by thermal variations both internal and external to the laser system, the laser does not supply a constant optical power. The power varies by $\sim 1\%$ on a time scale of seconds, and by up to 10% over periods of half an hour. A typical variation of the laser power over time is given in figure 1.4. The effect that drift has on the degree of squeezing is shown in figure 1.3. It is therefore required that the drift in power is controlled.

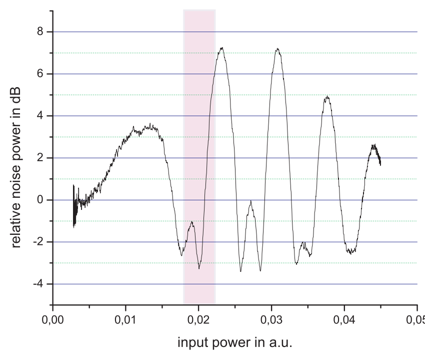

Figure 1.3: Squeezing as a function of input power, where 0dB corresponds to the uncertainty of a coherent state. The experiment normally uses the second minimum shown (0.02 in this example). The shaded area shows the region in which the NOLM might operate during the course of an experiment, if the laser power is not stabilised. The degree of amplitude squeezing can change from -3dB (noise variance is a factor of two smaller than the coherent state) to 6dB (a factor of four larger than the coherent state).

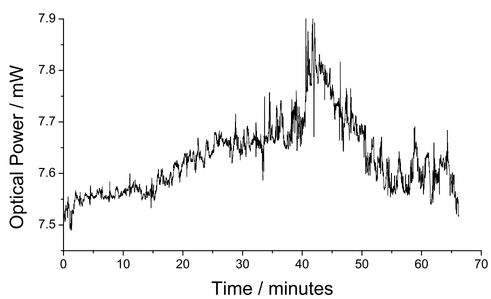

Figure 1.4: Typical example of the change in laser power over time.

1.2 Entanglement

In both classical and quantum physics, there is the possibility for systems to exhibit correlations. Classically, this might take the form of pairs of socks, whereby if the colour of one sock in a pair is measured, the colour of the other sock can be deduced without measurement. Quantumly, correlations can be demonstrated with electrons, whereby if the spin of one electron in a pair is measured, the spin of the other can be deduced without measurement.

Examples of such correlations could be written as

$$\begin{array}{ll} & |blue\rangle|blue\rangle \\ or & |\uparrow\rangle|\downarrow\rangle. \end{array}$$

Where the value in the first ket is the result of measuring the first observable. The result of a measurement on the second observable will be given by the second ket, with certainty. This measurement result can be known, even before a measurement is made.

In contrast to classical physics, quantum mechanics also allows systems to be in a superposition of states. For example, an electron can in some way be simultaneously both spin up and spin down, and does not need to "decide" which until it is measured. This could be written as

$$a|\uparrow\rangle + b|\downarrow\rangle. \tag{1.2}$$

In eq (1.2) the electron is in a superposition, and upon measurement will be spin up with probability $|a|^2$, and spin down with probability $|b|^2$. Once it has been measured, all subsequent measurements will be consistent with the first measurement, but the result of the first measurement is unknown.

Importantly, quantum mechanics allows superpositions of correlated states [2]. For example, a pair of electrons must have opposite spins, but until the spin of one is measured, they can exist in a superposition state. Such a state can be written

$$a|\uparrow\rangle|\downarrow\rangle + b|\downarrow\rangle|\uparrow\rangle. \tag{1.3}$$

The system does not have to decide in which state to be, until a measurement is performed. However, if a measurement is performed on the first electron, and a result of spin up is obtained (as it will be $|a|^2$ of the time), then all subsequent measurements on the system must be consistent with the system being in the first of the two states in eq (1.3). Any measurement on the second electron will therefore certainly give the result "spin down". The system cannot be treated as two separate subsystems, but rather viewed as a unit; a measurement on one electron effects both. Significantly, there is no reason that the electrons in such a state must be near each other; the effect is non-local. This effect, of non-local correlations of quantum states, is called entanglement. While the above example considered discrete variables (spin up/down), it is possible to generalise the notion of entanglement to continuous variables (e.g. momentum or position).

The group at Erlangen carries out experiments into continuous variable entanglement of amplitude and phase of light, for which the uncertainty in the phase and amplitude of two beams are correlated and anti-correlated, respectively. The accuracy with which the amplitude and phase of a given beam can be known is limited by the uncertainty principle. However, certain combinations of these variables in two subsystems can be known exactly, for example the total amplitude of the two beams and the difference in their phase. Using this fact, if the combined amplitude is known, and one beam is measured to have, say, an amplitude slightly lower than the expectation value, it can be stated with certainty that the second beam will have an amplitude a little higher than the expectation. These correlations are a witness of entanglement, and entirely quantum in nature.

Clearly, this accuracy of prediction will have wide ranging applications. One use is that of quantum interferometry, whereby the beams used in the two interferometer arms are entangled. Such a scheme can measure below the minimum error of classical interferometry

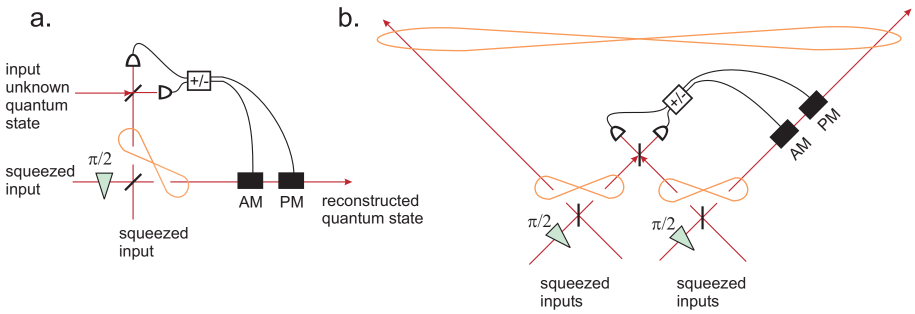

Figure 1.5: (a) shows the teleportation of an unknown quantum state. The measurement at the two detectors non-locally effects the lower entangled beam. Using the classical information obtained, here in the form of amplitude and phase modulations (AM and PM), it is possible to "work backwards" and reconstruct the unknown state. If the unknown state was originally entangled, the teleported state is also entangled (b) [13].

by a factor related to the quality of entanglement, and have been suggested for, for example, gravitational wave detection [17]. An interferometric setup can be extended to realise quantum dense coding, whereby the reduced noise allows the amplitude and phase modulations of a signal to be read with precision below the limit given by the Heisenberg uncertainty principle. For large photon numbers, this can increase the capacity of a telecommunications channel by a factor of two [18].

The non-locality of entanglement allows the quantum teleportation of an unknown quantum state, as shown in figure 1.5a. Here, two entangled beams are spatially separated, and the unknown quantum state is interacted with one of the beams. The outcome of this interaction is then measured, which fixes the state of the distant entangled beam. The results of the measurement are transmitted classically to the remaining entangled beam where the original unknown quantum state can then be reconstructed [13]. If the original unknown state was itself entangled with a fourth object, the process is termed entanglement swapping. By this method, two beams that have never interacted with each other can become entangled (figure 1.5b). Entanglement swapping has various applications including quantum communication protocols [19].

The accuracy of interferometry, the density of information coded, and the fidelity of teleportation all depend on the quality of entanglement. For continuous variables, however, perfect correlations cannot be achieved. The uses described above can only be achieved if at least some entanglement is present, and so some measure is required to say how strong the correlations must be for the two subsystems to be entangled.

If the amplitude or phase of a single beam is measured, the result can usually be known in advance to an accuracy bounded by the uncertainty principle, ie:

$$V(\hat{X})\,V(\hat{Y}) \geq 1 \tag{1.4}$$

where $\hat{X}$ is the amplitude quadrature of the beam,
$\hat{Y}$ is the phase quadrature of the beam,
V($\hat{A}$) is the variance of $\hat{A}$.

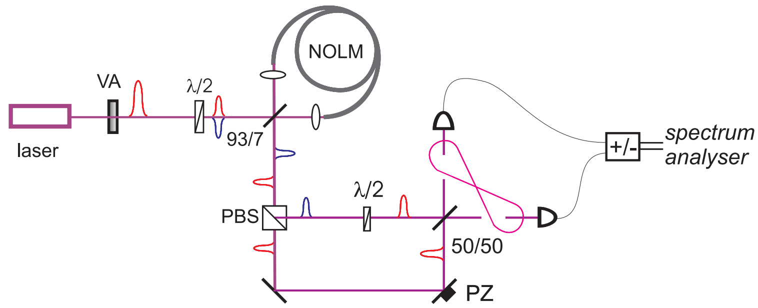

Figure 1.6: Optical train to give entanglement. The two squeezed beams produced by the NOLM (see figure 1.2) are interfered on a 50:50 beam splitter. This produces entanglement of bright beams [16].

Equality is achieved at the so-called "vacuum noise level".

With correlated beams, it is possible to measure one beam and infer some value for the variance of the amplitude of the second beam, $V_{inf}(\hat{X})$. A similar measurement and inference can then be made for the phase. For perfect correlations, and so perfect entanglement,

$$V_{inf}(\hat{X}) = V_{inf}(\hat{Y}) = 0.$$

A sufficient condition for two beams being entangled is the ability to infer $\hat{X}$ or $\hat{Y}$ to a precision below the vacuum noise level [20], ie:

$$V_{inf}(\hat{X})\, V_{inf}(\hat{Y}) < 1. \tag{1.5}$$

This does not violate the uncertainty principle as $V_{inf}(\hat{X})$ and $V_{inf}(\hat{Y})$ are not simultaneous; the amplitude is measured, and then the phase some time later. Importantly, between the two measurements, the underlying statistics of the system before measurement do not change.

Entanglement can be achieved experimentally using the train in fiugre 1.6. The two squeezed beams produced by the NOLM are interfered on a 50:50 beam splitter. The two output beams are thereby entangled. The entanglement quality depends on several factors. These include the degree of squeezing of the input beams, and the interference phase, ϕ [5]. Mechanical instabilities and air currents, which give rise to thermal variations, alter the optical path length on a time scale of seconds, and by distances of several hundred nanometres. This gives a drift in phase difference of $\frac{\pi}{2}$. The effect of this drift can be seen in the intensity of the output beams, as shown in figure 1.7. A phase change of this magnitude gives a variation in degree of entanglement between the maximum entanglement allowed by the quality of the squeezing, and no entanglement [16]. It is therefore required that the optical lengths of the interferometer arms, and thereby the phase at the beam splitter, be actively controlled. Ideally the control should be accurate to a few nm. This will give an error in the degree of entanglement below that due to imperfect squeezing.

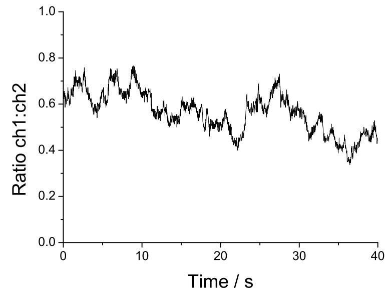

Figure 1.7: Typical ratio of the amplitudes of the two entangled beams over time. The drift is caused by changing interference phase.

1.3 Project aims

This project aims to stabilise the entanglement source currently used at the Centre for Modern Optics (ZEMO). This will be carried out in two parts. Firstly, the long term drift in laser power must be removed, thereby providing a source of bright beams with a constant, high degree of squeezing. Thereafter the phase difference in the interferometer arms must be controlled, to provide a source of consistently highly-entangled beams.

Chapter 2

Laser Stabilisation

2.1 Proposed stabilisation scheme

To control the laser power, a scheme was proposed by the group in Erlangen, which would fit in with the existing optical setup. The proposed scheme is shown in figure 2.1. The light emitted by the laser is p-polarised (p-pol, ie parallel to the optical table). The half-wave plate (λ/2) rotates this polarisation by an amount dependent on the orientation of the plate, and thereby alters the amount of light transmitted by the polarisation beam splitter, the reflected light being discarded. The amount of light transmitted is then monitored by reflecting a small fraction of the beam onto a detector, using a glass plate. The detector signal is fed back to a PC, which is able to control the angle of the wave plate via a step motor. The control loop can thus regulate the power of the transmitted beam, to a constant value.

The first aim of the project was to implement this proposed feedback scheme. Its implementation required that:

- a DC detector be designed and assembled;
- a control program be written to interface with the detector and step motor;
- the control loop be built into the existing optical train, shown in figure 1.6, in place of the variable attenuator.

2.2 Apparatus

The apparatus and components to be used for the project were chosen, taking several considerations into account. These included the components currently used by the group, ease of availability, ease of use, and cost. Naturally apparatus which the group already possessed was used where possible, and gross alterations of the experimental set up were avoided. Below is given an outline of the apparatus used, and a brief justification of the choices made. A full list of parts used is given in appendix A.

Computer

The computer used was a standard PC. It received signals from the detector via a National Instruments Analogue/Digital (AD) card, and controlled the step motor via the printer port.

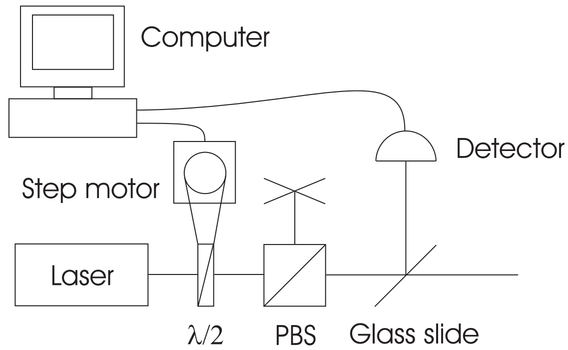

Figure 2.1: Proposed control scheme. The computer controls the amount of light incident on the detector by rotating the half wave plate ($\lambda/2$). This alters the proportion of light transmitted at the polarisation beam splitter (PBS). The transmitted light is monitored by the detector.

The control program was written using LabVIEW version 6i, as this is the standard language used by the group for measurement automation. The program could receive voltage measurements from the AD card, and write directly to the printer port.

Detector

The detector was made using a printed circuit board (PCB) and standard surface mounted device (SMD) components. These were used as their small size allows for more compact detector design, and improves the detector's electro-magnetic (EM) compatibility with other equipment. That is to say, that the possible signals received from and sent to other equipment via stray EM radiation were reduced. The detector should not have been troubled by Radio Frequency (RF) radiation, as it filters out the high frequency signal components. However, were the components too large, antenna effects may have caused problems whereby noise from other equipment interfered with the detector [21].
The photodiode used was a large area (0.5 mm diameter) InGaAs Photodiode. This is normally used for quantum noise measurements, because it has high quantum efficiency, ie most of the photons ($\gg 90\%$) incident on the active surface excite photoelectrons [22]. It was used for the DC detector as there was a ready supply.
The housing was made of steel to further improve the EM compatibility.

Other hardware

• **Step motor.** The step motor was a two phase step motor. It was controlled via the computer's printer port using an SMC 800 control card. It was chosen as it was inexpensive and easy to use.
• **Half wave plate.** A zero order, anti reflection (AR) coated, quartz half-wave plate was used. This was optimised for 1530 nm. It is not important that the wave plate is not optimised for the exact wavelength being used, as high extinction is not required. It is only important that the wave plate and PBS together give controllable variable attenuation.
• **Wave plate mount.** In order to reduce the angle by which the wave plate turned per motor

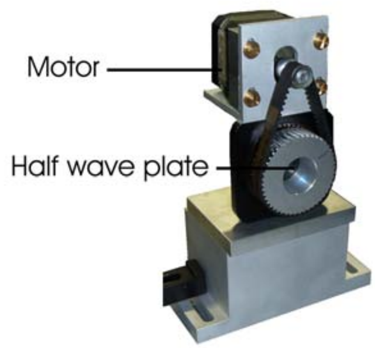

Figure 2.2: Mount for the motor and half-wave plate, showing the 1:5 gearing. The entire mount is 17 cm high.

step, the motor was attached to the wave plate via a 1:5 gearing ratio. The mount, including motor and wave plate is shown in figure 2.2. This was built in-house by the mechanics workshop.

• **Polarisation Beam Splitter.** Cubic PBS's are standardly used by the group. More than 98% of the incident p-polarised light is transmitted, with less than 0.1% of the incident s-polarised light (light polarised perpendicularly to the optical table) being transmitted [23]. The regulation is not disturbed by the reflected beam containing up to 2% of the incident p-pol light, as this beam is rejected. The mix of light polarisations in the reflected beam simply acts as a loss mechanism. The important point is that the transmitted beam contains as pure p-pol light as possible.

• **Glass slide.** This was a standard microscope slide. The exact fraction of light which was reflected out of the main beam was not critical.

• **Laser system.** This is a commercial system supplied by Spectra Physics. Light from a laser pumped Ti:Saphire laser is down-converted using an Optical Parametric Oscillator. It gives pulsed laser light at 1506 nm with a repetition rate of 82MHz and an average power of around 300 mW.

With the exception of the motor and half-wave plate, all components were mounted using the standard mounts used by the group.

2.3 Limitations of the apparatus

2.3.1 Overview of the limitations

There are two main factors that limit the accuracy with which the laser power can be controlled, namely:

- Resolution of the analogue digital (AD) card,
- Step size of the motor.

The AD card gives an absolute resolution limit (section 2.3.2), whereas the limit imposed by the step motor is proportional to the value being regulated (section 2.3.5). To achieve the smallest percentage fluctuations, the control scheme must work in the regime where the resolution is limited by the motor.

The finite step size of the motor gives finite steps in the transmitted power, and hence finite steps in the size of the detector output. The size of these steps depends on

- the optical power incident on the wave plate,
- the fraction of this light which is rejected by the control system, and
- the gain of the detector.

Taking into account the expected changes in incident power, the ideal fraction of light that should be rejected can be calculated (section 2.3.4). Conditions on the gain of the detector are then provided to ensure that the system operates in the regime of resolution being limited by the motor step size (section 2.3.6).

A value for the best possible control that can be achieved with the apparatus used is thereby given. In order for this to be realised, conditions are imposed upon the time scales in which the control loop must react (section 2.3.7).

2.3.2 Bit resolution of the AD card

The AD card has a range of voltages over which it can work. The user can select between a 5 or 10 Volt range, either starting at zero, or centred at zero. Over any of the four possible options this gives, the computer has 12 bit resolution, which is to say, it can recognise 4096 (2^{12}) distinct values [24]. The detector gives an output which is negative relative to ground, so the 0 to +5V range cannot be used. Thus the finest resolution of the detector card is achieved when the range $\pm$ 5 V is used. This results in the computer being able to resolve

$$\frac{10V}{2^{12}} = 2.5\text{mV} \equiv R_C. \tag{2.1}$$

Clearly the resolution of the AD card, R_C, is independent of the output voltage of the detector and, importantly, independent of the optical power incident on the detector. Thus while the absolute value of the resolution remains constant, for low incident powers the resolution steps, as a fraction of the measured power, are large.

2.3.3 Step size of the motor

The motor is designed to turn 1.8^o ($\approx$0.033 radians) per step [25]. It was linked to the half-wave plate via a 1:5 gearing ratio, making the angle turned by the half-wave plate:

$$\frac{0.033}{5} \approx 6.5\text{mrad per step.} \tag{2.2}$$

This is equivalent to 960 steps per full revolution of the plate.

2.3.4 Ideal operating power

The transmission of light through the wave plate and polarisation beam splitter (PBS) varies with the wave plate's angle as $\cos^2(2\theta)$. Towards the minima and maxima of the curve, the

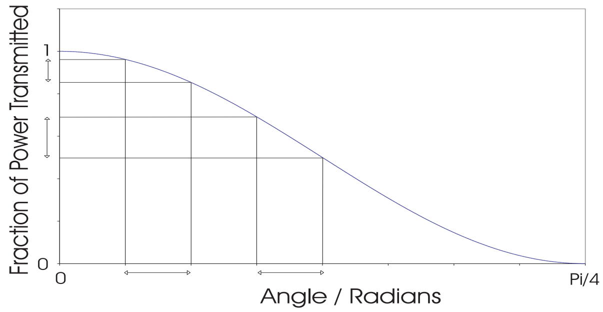

Figure 2.3: For a fixed change in angle, the change in transmitted power is smaller towards the minima and maxima of the curve.

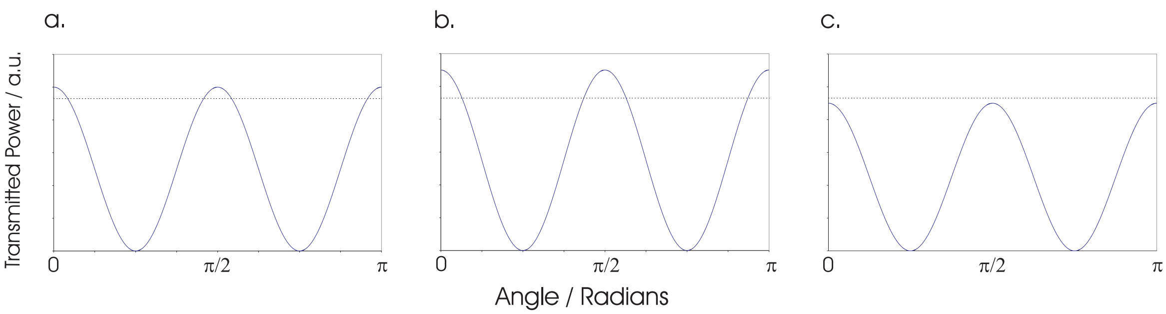

Figure 2.4: The Set point cannot be placed arbitrarily close to the maximum. To illustrate this, the dotted line is a possible, but poor choice of the set value. (a) shows the case of average incident power. If the power increases, the wave plate can turn so that the proportion of transmitted power is less (b). If the laser power decreases, there comes a point where there is no way for the set power to be transmitted (c).

gradient, ie the change in transmitted power per step, decreases, as illustrated in figure 2.3. This smaller change in power per step gives finer control, so ideally the system should work as close to the extremes of the curve as possible. When choosing between working close to a minimum or a maximum, the former option discards the majority of the light, whereas the latter transmits most of the light. For this reason, the set point should be put close to the maximum of the transmission curve.

The set point, however, cannot be placed arbitrarily close to the maximum, as the incident power varies. If the laser power increases, the half-wave plate can be rotated to transmit a lower proportion of the incident light (figure 2.4b). If the laser power decreases, the wave plate can rotate until 100% of the light is transmitted. If the laser power sinks still further, there is no way for the system to regulate to the ideal value, as shown in figure 2.4c. The set power must therefore be higher than the lowest power to which the laser is likely to drift. The laser used in the current experiment is known to drift by up to 10% over periods of half an hour.

Given that the power to which the system regulates, P_{reg}, should be as high as possible, while still being lower than the laser power is ever likely to reach, the set point was chosen to be 85% of the average incident power.

2.3.5 Power resolution per step

In the following calculations, the optical power incident on the wave plate, P_{inc} is taken to vary between P_{inc}^{min} and P_{inc}^{max}, with an average value of P_{inc}^{mid}.

If P_{inc}^{mid} is incident, then the optical power, P, transmitted by the PBS is described as:

$$P = P_{inc}^{mid} \cdot \cos^2 2\theta \tag{2.3}$$

where θ is the angle of the half-wave plate. The transmission curve at the chosen set point therefore has a gradient of:

$$\begin{aligned} \left.\frac{dP}{d\theta}\right|_{P_{reg}=0.85P_{inc}^{mid}} &= -4P_{inc}^{mid} \cdot \cos(2\theta) \cdot \sin(2\theta) \\ &= -1.43P_{inc}^{mid}\,\text{rad}^{-1}. \end{aligned} \tag{2.4}$$

The sign is not important here, it simply changes the direction in which the motor needs to turn. This is discussed in more detail in section 2.4.4. Putting the step size given in eq (2.2) into eq (2.4), the step motor has a power resolution of:

$$R_M = 9.3 \times 10^{-3} P_{inc}^{mid}\,\text{per step}. \tag{2.5}$$

From this it is clear that, unlike the resolution of the AD card, the step motor resolution is dependent on incident power. The resolution for high incident power is worse than for low incident power. This can be seen graphically from figure 2.5. This means that over the course of an experiment, the step resolution can be expected to have the mean value given in eq 2.5, but vary between $5.4 \times 10^{-3} P_{inc}^{mid}$ and $12 \times 10^{-3} P_{inc}^{mid}$.[1]

2.3.6 Operating voltage

The discrete steps taken by the motor will mean that, for constant incident power, the detector has discrete output voltages. Given any power resolution of the step motor, the size of the voltage steps given by the detector can be chosen arbitrarily by varying the amplification of the detector.

If the step size in the discrete outputs of the detector is very small, say 1 mV, then the motor will have to take 3 steps before the AD card registers any change. In this case the measurement is limited by the AD card. Conversely, if the step size of the detector voltage is larger than the AD card resolution, the detector will be the limiting factor. In the critical case where the resolution of the AD card and the step size of the detector output are equal, eqs (2.1) and (2.5) can be combined so that:

[1]These values can be reached by exactly the same method as used above, but using the extreme, rather than average, values. The full calculation is given in Appendix B.1.

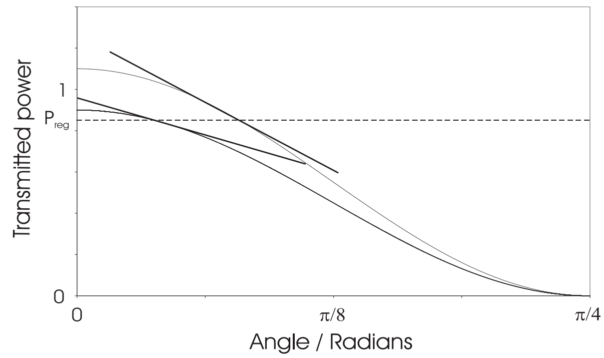

Figure 2.5: Transmission curves with P_{inc}^{max} and P_{inc}^{min} incident, showing the gradient of each at the ideal value, P_{reg}. The gradient of the P_{inc}^{max} transmission curve at the set power is steeper, and so the power resolution per step is worse, than at lower incident powers.

$$9.3 \times 10^{-3} P_{inc}^{mid} \longrightarrow 2.5\text{mV} \tag{2.6}$$

That is to say, a change in power of the size of the the motor's power resolution (eq 2.5) should cause the output voltage of the detector to change by an amount equal to the resolution of the AD card (eq 2.1).

In the standard running of the system, the amount of light transmitted to the rest of the experiment is P_{reg}=0.85P_{inc}^{mid}. From eq (2.6) then, in the critical case where the resolution limit of the AD card is equal to that set by the motor:

$$\begin{aligned} P_{reg} \quad & \longrightarrow \frac{0.85 \times 2.5\text{mV}}{9.3 \times 10^{-3}} \\ & \longrightarrow 0.23\text{V} \end{aligned} \tag{2.7}$$

Having calculated the critical case for P_{inc}^{mid} incident, the same can be done for the extreme cases of P_{inc}^{min} and P_{inc}^{max} being incident. As the amplification of the detector is linear, the resolution for the full range of amplifications, not just the critical amplification, can be calculated. The results of this are shown in figure 2.6.

The resolution limit of the AD card is an absolute, fixed value. The resolution of the detector varies as a function of incident laser power, and the amplification of the detector. Importantly, the resolution limit is proportional to the signal. As it is required that the fluctuations in laser power are small as a fraction of the power, the control system must work in the regime limited by the detector, and not the AD card. From figure 2.6 it can be seen that in order for this to happen over all expected incident powers, the amplification of the detector has to be such that the detector voltage, when P_{reg} is incident, is greater than 0.5 V.

Working above this threshold, the best possible sensitivity of the system is given by the gradient of the detector limit line. This is 1 $\pm$ 0.5% of the power, where the uncertainty is due to the different gradients for different incident powers.

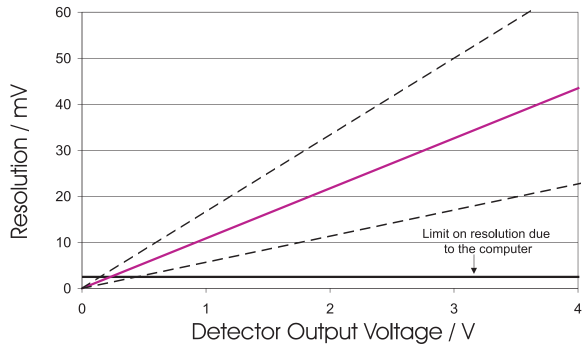

Figure 2.6: Graph showing detector resolution with average incident power (grey line) and extreme incident powers (dashed) as a function of the detector output voltage. For a fixed incident power, ie P_{reg}, this becomes a function of detector gain. The black line shows the constant AD card resolution.

2.3.7 Time resolution

The faster the system can react, the better, as it can then regulate away any deviation from an acceptable value as quickly as possible. Working above the 0.5 V threshold as calculated in section 2.3.6, the system can resolve fluctuations larger than 1%. It can thus be expected to regulate to the ideal value $\pm$ 0.5%. In order to realise this limit, the control loop needs to react quickly on time scales over which fluctuations of this magnitude occur. From figure 1.4 it can be seen that fluctuations of magnitude 0.5% do not occur over time scales shorter than 10 seconds. If the regulation system reacts more slowly, it is possible that the system would miss the fluctuations, or react after the event.

2.3.8 Conditions of optimal control

The above calculations have shown that the apparatus being used can, in principle, control the power to within 0.5% of the set value. This can be realised only if the detector signal is amplified such that the ideal value to which the computer must regulate is greater than 0.5V. It is also necessary that the entire feedback loop, comprising detector, computer and motor, can react in times much shorter than 10 seconds.

2.4 Computer control

The aim of the computer program was that it allowed the computer to rotate the wave plate so as to ensure that the detector always measured a power close to the ideal. In practice, the computer took a measurement from the detector and compared it to the ideal value it had been given. If the detector signal was outside specified tolerances, it moved the motor either left or right to compensate. The decision process of the program is shown in figure 2.7.

The control program essentially consisted of a main program called *feedback*. This co-ordinated the actions of two other sets of programs called *measurement*, which carried out the task of boxes 1 to 4 in figure 2.7, and *steps*, which collectively carried out boxes 5a and

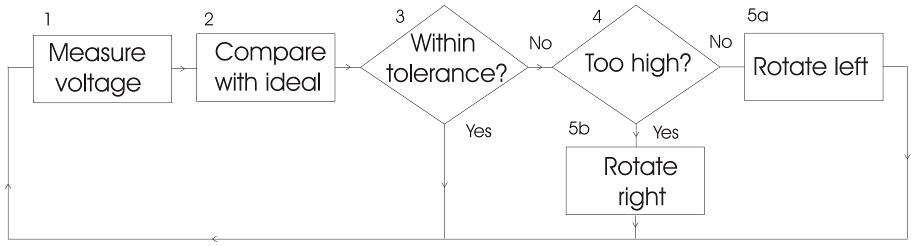

Figure 2.7: Flow diagram showing the basic form of the control program.

5b. *feedback* was then responsible for coordinating these actions. LabVIEW terms the main program a "*vi*". Any self-contained program on which a *vi* calls is named a "sub*vi*". Pictures of the code for each program are shown in appendix C.

The most complicated part of the program was *steps*. In order to understand these, a little background on the working of the step motor is required.

2.4.1 Step motor

The step motor used had four inputs, which controlled the current in four coils, which in turn moved the motor. The direction of rotation depended on the amount of current in the coils, which could take discrete values between 0 and 100%, and the phase of the current during each of two control phases. The four inputs were not entered directly, rather the control card was sent a binary string of eight digits, and the card then converted these into the inputs required by the motor.

The function of each of the control bits is summarised as follows:

Pin number	Function
1	Controls the amount of current sent
2	
3	Controls direction of Phase current, Phase A
4	Controls internal current
5	
6	Controls direction of phase current, Phase B
7	Motor Selection
8	

The exact details of what each bit means are not important here, except for the values of bits 7 and 8. The card had the potential to independently control 3 motors; the first six bits were for the motor control, the last two bits then dictated to which motor the first six bits were sent. For the laser stabilisation, only one motor had to be controlled, though in the event that future experiments require several beams to be controlled, or if the card is damaged so that one motor control does not work, it would be useful to be able to change the motor number. Bits 7 and 8 control the motor number as:

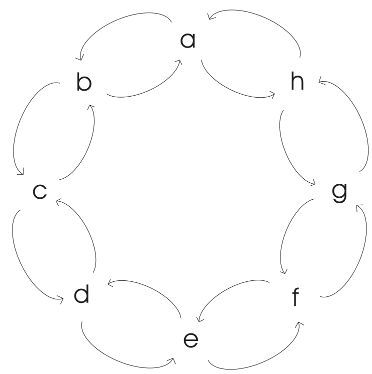

Figure 2.8: Order in which the states had to be sent. The motor moved right if sent states in a clockwise sequence, or left if sent them in an anti-clockwise sequence.

Bit 7	Bit 8	Motor controlled
0	0	1
1	0	2
0	1	3

Not counting the choice of motor from the last two bits, there are 8 different states that can be sent to the motor. The control bit values for the eight states are given in appendix C. These were termed *steps a - f* for historical reasons, though a more accurate name would be *states a - f*. One individual state did not change the position of the motor. Rather the motor was moved by changing from one state to another. Thus if state *d* was sent initially, the motor would do nothing, but wait for the next state. If it was subsequently sent state *c*, it would rotate right, and if it received state *e*, it would rotate left. By convention, when looking towards the motor along the spindle, "left" is used to describe an anti-clockwise rotation and "right" a clockwise one. The sequence of states then continues in a circle, as shown in figure 2.8.

It was possible to send only every other state (for example, state a, then c, e and g.) This increased the speed of the motor, at the cost of larger step size.

The control bits are sent via pins 2 - 9 of the printer port. Pin 1 is then used as a strobe signal. When the strobe is turned off, the card reads off whatever states the printer port pins are in.

2.4.2 Steps

There were eight separate *step* sub*vi*'s. Each of these contained the eight control bits needed to send one of the states *a* to *f* to motor number 2. When a *step* sub*vi* was called, it turned the strobe signal on, sent its eight control bits to the printer port pins, and then turned the strobe signal off.

The eight control bits were entered as an array of 8 buttons to turn on or off, to correspond to a 1 or 0 respectively. The computer then treated this as a binary number, where the first button is 2^0, the second 2^1 and so on, up to 2^7 for the last button.

The default step contained control bits that would send a given state to motor 2, ie the last two bits, which dictate the motor, are “1 , 0”. An option on the front panel of the program allowed the user to chose between controlling motors 1, 2 or 3. The program could select motors 1 or 3 by adding or subtracting 64 (ie 00000010) from the default state.

2.4.3 Measurement

measurement carried out the tasks of boxes 1 to 4 in figure 2.7. The sub*vi* took 3 numbers as input, namely the ideal value and the tolerance within which it has to work, both of which were specified by the operator, and the output signal from the detector. It then gave two logic values as output. These were “too high” and “too low”.
Both outputs are set to false (ie ¬ “too high” and ¬ “too low”) if the condition

$$|\text{ideal value} - \text{measured value}\,| < \text{tolerance} \tag{2.8}$$

was fulfilled. If this inequality was broken, that is, if the measured value varied from the ideal by more than the allowed tolerance, then the program checked whether the measured value was larger or smaller than the ideal. Depending on whether the measured value was too high or too low, it set one of the two outputs to true, and the other to false.

If *measurement* had no tolerances, the motor would never remain stationary, but step either left or right at every iteration of the program. Each step it would allow just too much or just too little light to be transmitted. This would produce a periodic step in the laser power (figure 2.9a). Assuming the laser power drift between steps is small compared to the step size this gives an error twice as large as the step size. In order to keep these errors small, a tolerance must be introduced. If the tolerance is smaller than the step size, then for some periods the motor will remain stationary, while for others it will continue to step back and forth, over-stepping the tolerance each time (figure 2.9b). To ensure that the motor never oversteps, and so never oscillates, the tolerance must be set so that it is greater than or equal to the motor’s step size. The above results, assuming that the drift between steps is small, are summarised in figure 2.10: for zero tolerance, the error is twice the step size. It decreases linearly until the tolerance equals half the step size, and then increases as the tolerance continues to get larger.

As the step size is dependent on the incident power, the tolerance should be set to the step size when P_{inc}^{mid} is incident on the wave plate. This ensures that the accuracy is kept to a low value for all incident powers.

2.4.4 Feedback

feedback took the truth values given by *measurement*, and decided which states needed to be sent to the motor. The initial decision as to which of boxes 5a and 5b lead to stepping left or right was not critical. If stepping left actually decreases the power, then the program would continue iterating round the loop turning further and further left until the power was within tolerance, as shown in figure 2.11. The program may do this once when it was first started, but once it was on the correct slope of the transmission curve, it regulated properly.

As can be seen from section 2.4.1, in order to send the correct step, the program had to know which step has been most recently sent. *feedback* did this by keeping a tally. For every

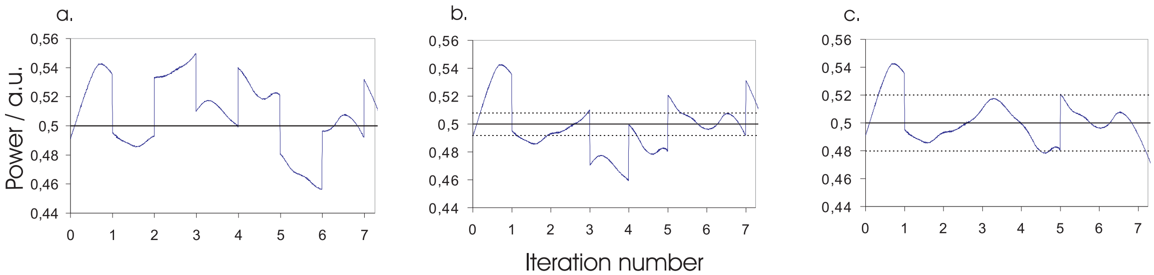

Figure 2.9: Model that controls drift to a set value (0.5), within set tolerances (dashed lines). With no tolerance (a) the the motor moves at every iteration of the code. With small tolerances (b) it is possible that the motor remains stationary, but it can also undergo periods of overstepping. If the tolerance is greater than half the step size, and assuming that the drift in laser power per iteration is small, then the motor does not overstep (c).

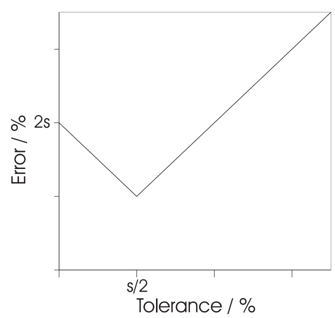

Figure 2.10: Error (the distance between the bounding lines of the errors, as in figure 2.9) as a function of the tolerance. The smallest error is achieved when the tolerance equals half the step size, s/2. This can also be seen in figure 2.9: the error is smaller for larger tolerances, up to s/2 . This graph was drawn using the assumption that the drift is very small on the scale of time between steps.

step it turned left it added one to the tally, and for every step right, it subtracted one. By counting in this way in modulo eight, it could keep track of which step was last sent, and hence which step had to be sent next to turn the motor in the desired direction.

2.4.5 Constant rotation

The power that needs to be coupled into the fibre in order to achieve squeezing is always constant and depends only upon the NOLM (see section 2.5.3). However, from day to day the coupling efficiency into the fibre changes, and thus the amount of light that must be incident on the fibre end in order to achieve squeezing varies. It is therefore not possible to simply say that P_{reg} must be some value and that this remains constant for all situations.

To find the value of P_{reg} for a particular measurement run, it is useful to be able to scan through a range of powers and see at what power the maximum squeezing is achieved.

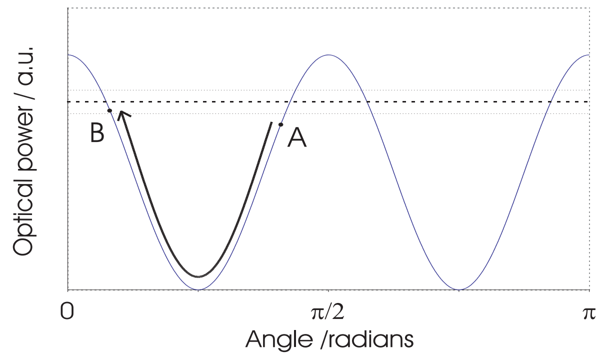

Figure 2.11: Initially, the power is too low (A). The computer then turns the ”wrong” way, but continues until it is within tolerances (B). Thereafter, it operates as normal.

To allow the LabVIEW program to do this, an extra layer was added above *feedback*, which enables the user to choose between regulation, whereby the computer controls the transmitted light to a fixed value, and rotation, whereby the the motor constantly turns, so as to scan the power incident on the fibre over the full possible range.

This top layer was named *control*. In the “regulate” mode, *control* calls *feedback*, and *feedback* works exactly as before. In the “rotate” mode, *feedback* is called, but unlike before, is not sent the signal from the detector. Instead it is told that the detector signal is 1000V. *feedback* then turns the motor until it is told that that the detector signal is within the set tolerance. Clearly, as the the motor turning does not effect the number that *feedback* is given, the motor carries on turning until the user stops it. A toggle switch allows the user to chose between the motor rotating either right or left. If the motor must rotate left then *feedback* is told that the detector signal is -1000V.

2.4.6 Use of pauses

The computer program was executed, then returned to the beginning and re-run. The maximum speed at which the motor could turn is approximately one step every 10 ms. If states were sent faster than this, the motor simply stopped. In order for the motor to turn, therefore, the code had to take more than than 10 ms to run. *feedback* on its own ran faster than this, and so pauses were added, whereby the program was run, waited for a specified time, and then re-ran. If *feedback* was used as part of *control*, then the extra time needed for the additional code negated the need for pauses. The pauses were not removed from the program all together as they could be used to alter the speed of rotation under the “constant rotation” mode. Naturally, the maximum speed of the motor when using *control* was obtained when the pauses are set to zero.

The highest speed at which the program can turn the motor was 12.5 ms per step. This fulfilled the criterion in section 2.3.7 that the control be fast compared to 10 seconds.

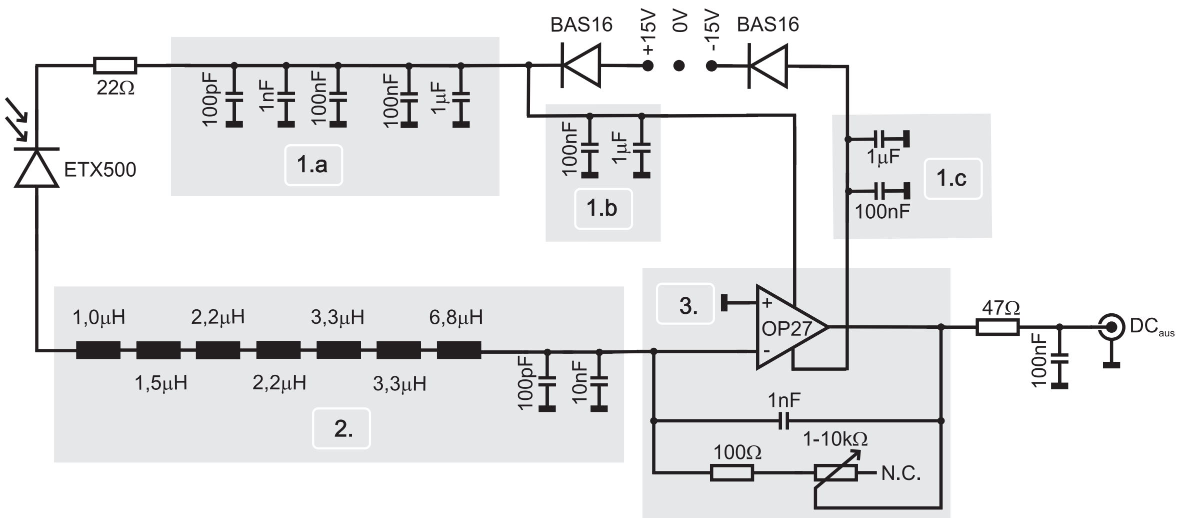

Figure 2.12: DC detector circuit.

2.5 DC detector

The group already had a combined AC/DC detector, developed by M. Langer [26]. Several detection systems used by the group require only DC detection. Building a dedicated DC detector that could be used for these had several advantages over using a general detector. Requiring fewer components, a DC detector would be cheaper and smaller, thereby saving space on the optical table. They are also less complicated and so could be more easily optimised specifically for DC measurements.

The combined detector had two very distinct parts, one for filtering out the AC part of the signal to give a DC output, and the other for filtering out the DC part to leave the AC signal (see appendix D). The combined design was modified, essentially by removing all components that were used for AC detection or for filtering out the DC signal. The design arrived at by this method is shown in figure 2.12. A printed circuit board was then designed using EAGLE (Easily Applicable Graphical Layout Editor) Version 4.01, so that the design could be built using SMD components. The PCB layout is shown in appendix D.

2.5.1 Operation of the detector

From figure 2.12, part (1a) is a low pass filter, to ensure that the DC voltage from the voltage supply really is DC. The impedance, Z, of a capacitor, C, is given as:

$$Z = \frac{1}{j\omega C}$$

where ω is the frequency of the signal. The filter therefore provides a very high impedance path to ground for the DC components of the signal, while the high frequency components are earthed. Several capacitors were used, rather than one with the equivalent value, as this reduces the tolerances.

Parts (1b) and(1c) are low pass filters to ensure that the voltage that powers the operational amplifier is free of high frequency noise.

Part (2) is a low pass filter to remove high frequencies from the photodiode signal. The impedance of an inductor, L, is given as:

$$Z = j\omega L.$$

Thus the high frequency components have a large voltage drop across the inductors, while there is very low resistance to the DC signal. The capacitances earth high frequency components, as in part (1).

Part (3) is an amplifier and low pass filter. The capacitor and resistor between the output and the inverting input of the operational amplifier (op-amp) provide a feedback loop. The gain of the op-amp is proportional to the feedback impedance. Thus high frequencies, which see a very low impedance across the capacitor, are very weakly amplified. The amplification of low frequency signals, which see a large impedance across the capacitor, can be adjusted using the variable resistor. The 3dB frequency of the amplifier, ie the frequency amplified only half as strongly as the DC signal, is [27]:

$$\omega_0 = \frac{1}{C \cdot R} \tag{2.9}$$

where C is the capacitance, and R is the resistance between the output and inverting input. ω_0 is can be varied as R is a potentiometer. The minimum value for the component values used is 100kHz.

2.5.2 Detector response

The frequency response of the entire detector was modeled using the program WIN-Electronic. The circuit was modeled as shown in figure 2.13. Except for the photodiode and voltmeter, the model detector should have exactly the same behaviour as the actual detector, the only difference being that the individual components were combined to give the effective value of the group of components.

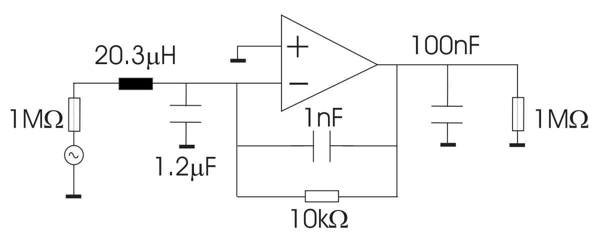

Figure 2.13: Model of detector used to calculate the frequency response. The voltage source and resistor on the left behave similarly to a photodiode. The 1 MΩ resistor on the right behaves similarly to a voltmeter. The component values used for the rest of the circuit were the effective values of the groups of components in the physical detector.

The photodiode should approximate to an ideal current source [28]. It was modeled as an ideal voltage source in series with a large resistance (1 MΩ). The voltmeter, or computer, ideally has an infinite impedance. In the model a resistance of 1 MΩ was used. These approximations should hold provided

$$Z_D \ll 1M\Omega \tag{2.10}$$

where Z_D is the impedance of the detector circuit, not including the photodiode.

It is worth noting that at DC, the capacitors have very high impedance. The only part of the detector then connected to ground is the non-inverting input of the op-amp. The condition in eq (2.10) can still be met, however, as there is a virtual short circuit between the inverting and non-inverting terminals of the op-amp [29].

The theoretical frequency response curve is shown in figure 2.14. The 3dB point for the entire detector is 28kHz. This is faster than the laser fluctuations that will be measured, and ensures that very high frequency signals are suppressed.

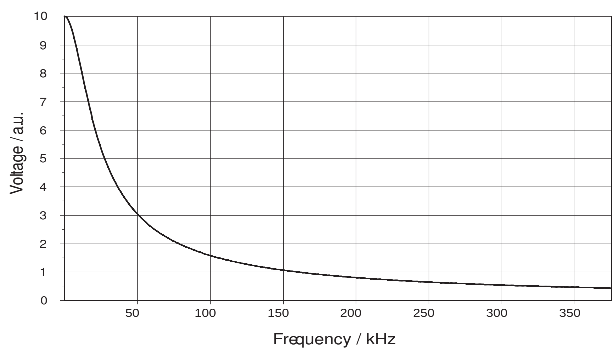

Figure 2.14: Frequency response of the model detector shown in figure 2.13. 3dB frequency is 28kHz.

2.5.3 Detector gain

From section 2.3.8, the detector had to give an output signal of greater than 0.5V if the ideal control was to be attained. The minimum value of P_{reg} was fixed by the NOLM: the power coupled into the fibre had to be that of the first squeezing minimum. This power was dependent upon the non-linear properties and the length of the fibre. It can therefore vary between NOLMs, but for any given NOLM it has a fixed value. For the NOLM used in the present experiment, the first squeezing minimum occurred at $\sim$ 3.5 mW. The fibre simultaneously squeezed two orthogonal polarisations, and had an input coupling efficiency of $\sim$ 75%. The light that must be incident on the fibre end was therefore:

$$\frac{3.5\text{mW} \times 2}{0.75} \approx 9.5\text{mW} \tag{2.11}$$

The amount of power that must be incident on the detector, however, was not dependent on this value. By using attenuators either before the NOLM or before the detector, the two powers could be totally independent. During an experiment the maximum optical power that could be incident on the detector was 2mW, where the limit is set by the output of the laser.

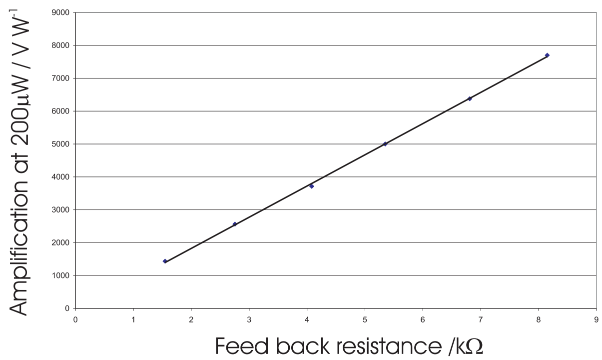

Figure 2.15: Gain of the detector with 200 μW incident on the photodiode as a function of feedback resistance.

To get a high enough voltage signal from the detector, for a normal incident power, several feedback resistances were tested and gave values of gain as shown in figure 2.15. A 1-10 k Ω variable resistor was used in series with a 100 Ω to provide a useful working amplification. The 100 Ω resistance was negligible compared to that of the potentiometer and is not required. It was left from the original design, and was not worth removing. For ease of conversion, the feedback resistance was set to 5.35 kΩ. This gave an amplification of 5000 V/W. This meant that 100 μW incident light gave a 0.5 V detector signal.

2.5.4 Linearity

For the purposes of the project, it was not essential that the detector response was linear, only that it be bijective. However, if it could be shown to have a linear response, the detector then becomes more useful for general applications. The response was tested using the train illustrated in figure 2.16

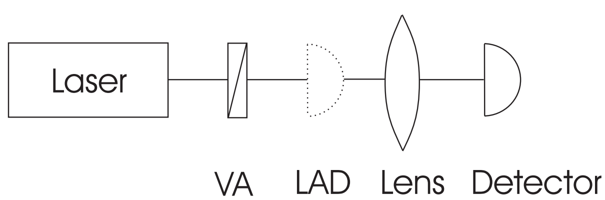

Figure 2.16: Optical train to test the linearity of the detector response, comprising a variable atenuator (VA), removable large area detector (LAD), lens, and the detector under test.

The large area detector (LAD) was inserted into the beam, and the variable attenuator (VA) adjusted until the required optical power was transmitted. The LAD was then removed and the detector reading taken. This was repeated over a wide range of powers. The results are shown in figure 2.17.

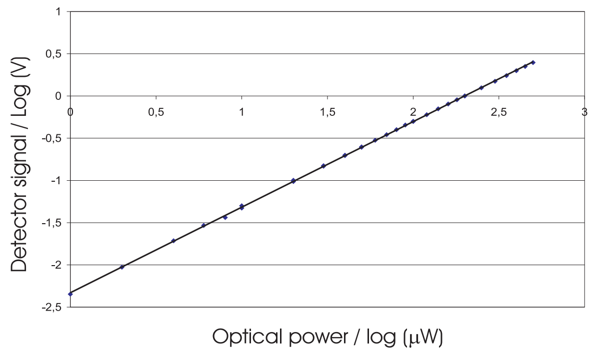

Figure 2.17: Detector signal as a function of the incident optical power with a feedback resistance of 5.35kΩ.

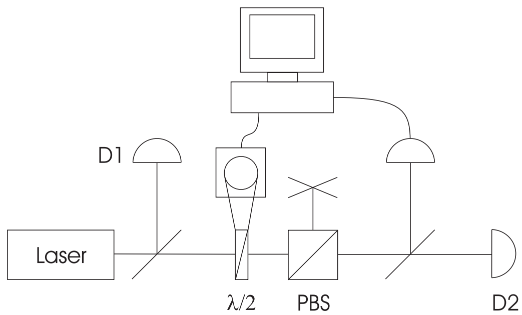

Figure 2.18: Optical train used for testing the stabilisation scheme. (See figure 2.1 for details of function.)

2.6 Testing of the power stabilisation

2.6.1 Method

A train to demonstrate entanglement swapping had been built, and the power stabilisation setup would be added to this. It was therefore not possible during the project to test the effect of power stabilisation on squeezing directly. Instead, the arrangement shown in figure 2.18 was built, whereby the value of the transmitted power was measured directly by detector 2, rather than the light being coupled into the NOLM. The effect on squeezing of the measured power power variation was then calculated.

The parameters discussed in section 2.3 were set so that

$$\begin{aligned}
P_{inc}^{mid} &= 8.5\text{mW} \\
P_{reg} &= 7.34\text{mW} \\
V_{reg} &= 0.65V \\
\text{Tolerance} &= 5\text{mV} = 0.77\% V_{reg}
\end{aligned}$$

The power was recorded at D_1 and D_2 over time, and the results are shown in figure 2.19.

Measurements were then taken using smaller values of the tolerance, the smallest being 1.5mV (one fifth the step resolution), to test the prediction made in section 2.4.3 that the tolerance must be greater that half of the step size. The results of the tests with smaller tolerances is shown in figure 2.20.

2.6.2 Results

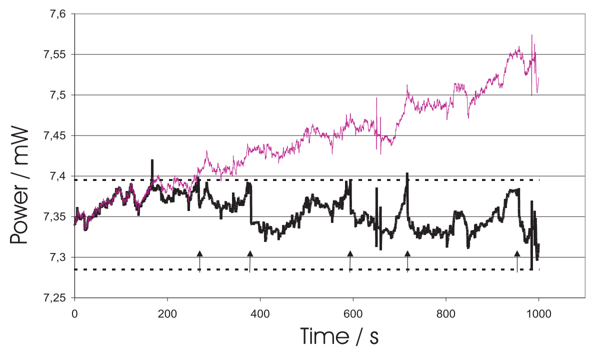

Figure 2.19: Laser power measured at D_1 (grey) and D_2 (black). The dashed lines show the size of the tolerance ($\pm$0.75%). The arrows show the points at which the motor moved. For ease of comparison the monitor signal (D_1) has been linearly scaled so as to start at the same power as the transmitted signal (D_2).

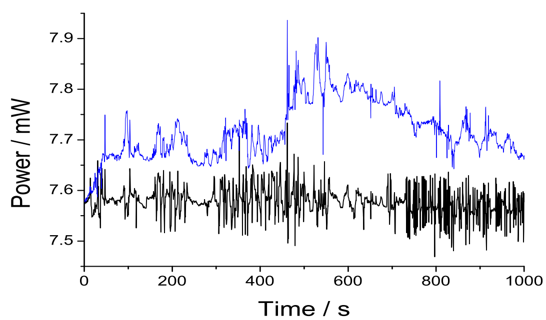

Figure 2.20: Power stabilisation with a tolerance equivalent to 0.25% of the transmitted power. As with figure 2.19, the monitor (grey) has been scaled to start at the same power as the transmitted signal (black)

The step size can be seen from graph 2.19 to be 0.7 $\pm$ 0.1%. The power is controlled to within 0.75% of the ideal. As predicted, the factor that limits the precision of the stabilisation is the tolerance set, shown by the dashed lines.

When the tolerance is set to be smaller than the step size, the motor steps back and forth, as in figure 2.20. The precision of the control in this case is $\pm$0.8%. Using the model in

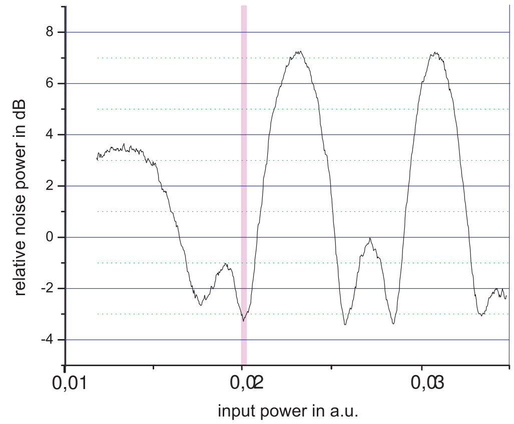

Figure 2.21: Degree of squeezing as a function of input power. Using the stabilisation system, the power can be held constant to within the shaded region. This can be compared to figure 1.3 which shows the range of squeezing achieved without power stabilisation.

section 2.4.3, and the values given above, a value of $0.9 \pm 0.2\%$ would be expected, where the uncertainty comes from the uncertainty in the step size.

Figure 2.21 shows the effect of the size error in figure 2.19 on the degree of squeezing. It can be seen that the squeezing can be kept within 0.5 dB, or 12%, of the maximum. This can be compared to figure 1.3, showing the effect of the uncontrolled drift on squeezing.

Chapter 3

Phase Regulation

3.1 Proposed regulation scheme

To control the interference phase, it was proposed that the brightness of the two entangled output beams be monitored, and their ratio used as a measure of the interference phase. Maximal entanglement is achieved when the phase difference of the input beams is $\frac{\pi}{2}$ [5]. The ideal case is therefore realised when the incident beams interfere so that the output beams are of equal brightness, or more accurately, have the same classical field amplitude.

To regulate the brightness of the beams, it was proposed that the DC signals from the detectors be used as monitor signals. The difference between the two output voltages should found electronically, and a controller of some form be used to regulate the difference to zero. The controller changes the position of the piezo, and hence the path length. The proposed system is shown in figure 3.1.

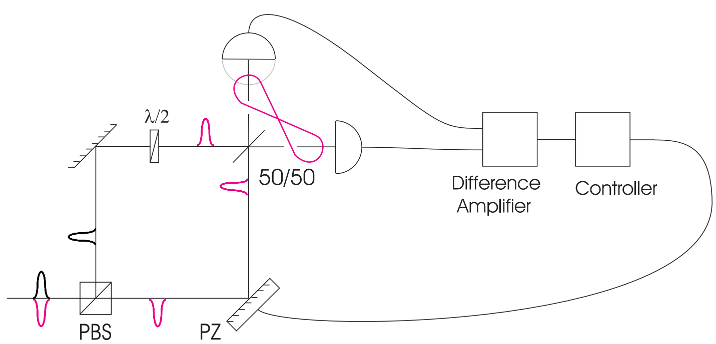

Figure 3.1: Proposed control loop. Two orthogonally polarised, amplitude-squeezed beams from the NOLM are separated at a polarisaton beam splitter. One beam's polarisation is rotated by 90^o by a half-wave plate, so that the two beams can be interfered on a 50:50 beam splitter The output beams are thereby entangled. The phase can be monitored by measuring the difference in brightness of the two entangled beams. The controller then changes the path length, and thereby the interference phase so as to regulate the difference in brightness to zero.

The beams being regulated contain both quantum and classical fluctuations. The quantum fluctuations are anti-correlated and are required to demonstrate entanglement. The classical fluctuations are from variations in the optical path length. While the phase regulation aims to suppress fluctuations, it must be noted that the regulation will not, indeed cannot, suppress the quantum anti-correlations being measured. This limit, that the quantum fluctuations cannot be suppressed, is important in that it means that the regulation scheme will not, in an attempt to stabilise the entanglement, degrade the anti-correlations being measured. Once this is noted, the quantum fluctuations can be ignored in the planning of the phase stabilisation, as they are much smaller ($\sim$7 orders of magnitude) than the classical fluctuations.

Fortunately, the variations due to technical difficulties do not have to be close to the quantum limit before entanglement can be accurately measured. Quantum fluctuations give white noise, ie, they occur at all frequencies. The technical noise occurs at different frequencies depending on the source: thermal drift occurs at frequencies of Hertz; the thermal noise of the detectors decays as $\frac{1}{f}$, so is negligible above 10 MHz; the repetition rate of the laser gives a very large frequency component at all multiples of 80 MHz. So as to not be saturated by this repetition peak, the detectors heavily suppress all signals above 35 MHz. There is therefore a region between 10 and 35 MHz that is effectively free of technical noise, and to which the detectors are sensitive [30].

The degree of entanglement can therefore be held near the maximum value using amplitude of the entangled beams to monitor the interference phase, without detracting from the results being measured. While it is not possible to reduce the technical noise to the level of the quantum noise, this does not hinder the entanglement measurement.

The second aim of the project was to implement this proposed feedback scheme. Its implementation required that:

- A differential amplifier be made,
- A suitable controller be designed and assembled,
- The control loop be built into the existing interferometer.

3.2 Apparatus

3.2.1 Differential amplifier

A differential amplifier takes two voltages, V_1 and V_2, as input. Its output, V_o, is proportional to the difference between the input voltages. A circuit which has this behaviour can be made using an operational amplifier (op-amp) as shown in figure 3.2.

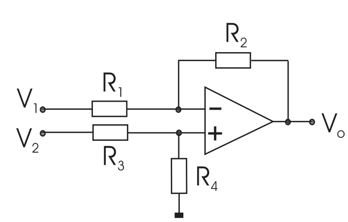

Figure 3.2: Schematic of a differential amplifier [31].

The response of the differential amplifier shown above is given by [32]:

$$V_o = \frac{V_2 \cdot (R_1 R_4 + R_2 R_4) - V_1 \cdot (R_2 R_3 + R_2 R_4)}{R_1 \cdot (R_3 + R_4)}. \tag{3.1}$$

Thus the circuit faithfully gives V_o proportional to the difference between V_1 and V_2 when

$$\frac{R_2}{R_1} = \frac{R_4}{R_3} = A \tag{3.2}$$

where A is the constant of proportionality. As the gain of the amplifier did not have to be large, the component values were chosen as:

$$R_1 = R_2 = R_3 = R_4 = 1k\Omega$$

All resistances had a tolerance of $\pm$ 1%. For the remainder of the report, it will be assumed that $R_3 \equiv R_1$ and $R_4 \equiv R_2$.

3.2.2 Controllers

There are several commonly used electronic control circuits, notably Proportional (P), Integral (I), and Differential (D) controllers. These give, respectively, a control signal proportional to the deviation from the ideal value; a signal which is the time integral of the deviation from the ideal value; and a signal related to the rate of change of the signal from the ideal value. It is possible to combine these systems linearly to give, for example a PID-controller. This would give a control signal of the form [33]:

$$u(t) = K_R \left(\underbrace{e(t)}_{P} + \underbrace{\frac{1}{T_N} \int_0^t e(t') \cdot dt'}_{I} + \underbrace{T_v \cdot \frac{d}{dt} e(t)}_{D} \right) \tag{3.3}$$

where: u(t) is the control signal given by the PID controller,
e(t) is the difference between the signal being controlled and the ideal,
K_R is a constant of proportionality,
T_N and T_V are time parameters of the controller.

The different possible combinations each have various advantages and disadvantages.

P-controllers.

Once the signal is disturbed from the ideal, P-controllers can return rapidly to a value which is close to the ideal, but displaced by an amount related to certain response parameters of the feedback loop and K_R. This distance by which it misses the ideal can be made small by choosing K_R to be large. However, for large values of K_R the P-controller becomes unstable. There will therefore always be some margin of error using realistic components.

I-controllers.

I-controllers are capable of returning to the exact ideal value. However they do so only slowly. The rate can be increased by the choice of components, but again, this can lead to problems of instability. This does not present difficulties if the signal is only expected to drift slowly away from the ideal.

PI-controllers.

PI-controllers return to the ideal value quickly, due to the contribution from the P-control. After the initial rapid correction, they also regulate to the exact ideal value, due to the contribution from the I-control. They are also less inclined to instability than P- or I- controllers on their own.

PID-controllers.

PID-controllers are very stable, rapidly get close to the ideal value, and can fine tune it to the exact value. However, they do not work effectively with a noisy input signal. The fast fluctuations from noise (as would be present with the detector signals that will be used) cause the D-control to give a very large response, which increases, rather than suppresses, the noise in the system.

3.2.3 PI-control

From the above outlined considerations, it was decided to use a PI-controller. This can be done using an op-amp as shown in figure 3.3.

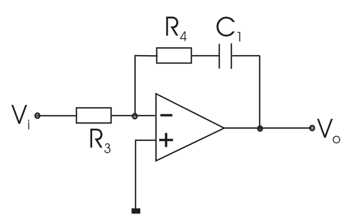

Figure 3.3: Schematic of a PI controller. [34]

From eq (3.3), the behaviour of the PI-controller is characterised by the two constants K_R and T_N. These are given by [35]:

$$K_R = \frac{R_4}{R_3}$$
$$T_N = C_1 \cdot R_4 \tag{3.4}$$

where R_3, R_4 and C_1 are as defined in figure 3.3.
The controller reacts more quickly for smaller values of T_N. The lower bound on the size of T_N is set by the speed of response of the system being controlled. This sets a upper limit on

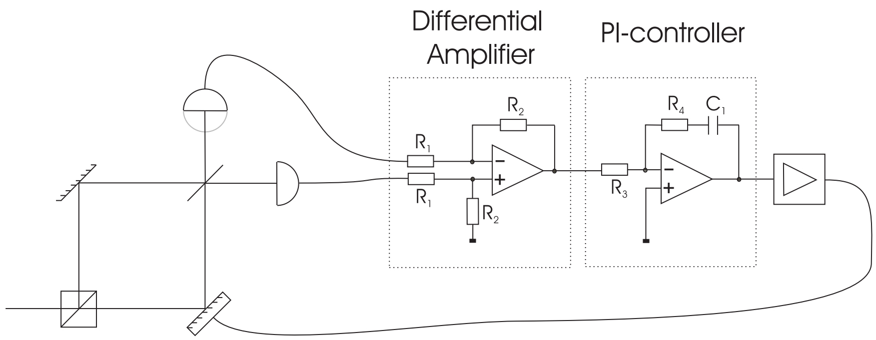

Figure 3.4: The complete proposed control loop, as described in figure 3.1, showing the electronic circuit of the differential amplifier and PI controller.

how fast the system can, in principle, be controlled. Significantly, while the fastest speed that the controller could correct is related to the speed of response of the uncontrolled system, it is in fact faster than the response of the uncontrolled system.

3.2.4 Control system

The system devised above takes the DC signal from the two detectors and calculates the difference. It then uses this difference signal as input for a PI-controller. This provides a feedback signal, which is amplified and used to control the position of the piezo. The movement of the piezo alters the path length, and hence the interference phase at the beam splitter. The electronic circuit required is shown in figure 3.4. This is the same setup as shown in figure 3.1, though the details of the differential amplifier and PI-controller have been added. The feedback loop should so work that the piezo ends at a stable displacement, at which the detector signals are equal.

3.3 First controller

3.3.1 Choice of parameter values

To set the ideal values of T_N and K_R, the response time of the system must be known. This would enable the interferometer to be controlled as quickly as possible, irrespective of how fast the control was required to be. Before carrying out a complete characterisation of the interferometer, a differential amplifier and PI-controller were built to show that in principle the control scheme would work. A value of $T_N = 1s$ was chosen. This was the time scale on which drift was observed, and so the time scale of the fluctuations that needed to be suppressed. The chosen parameters were then:

$$\begin{aligned} T_N &\approx 1\text{s} \\ K_R &\sim 1 \end{aligned}$$

The following component values were therefore used:

$$\begin{aligned} C_1 &= 0.1\mu\text{F} \\ R_3 &= 1.5\text{k}\Omega \\ R_4 &< 10\text{k}\Omega \end{aligned}$$

where the inequality denotes the use of a variable resistor.

3.3.2 Testing of the first controller

The control setup shown in figure 3.4 was built, and tested. The results are shown in figure 3.5.

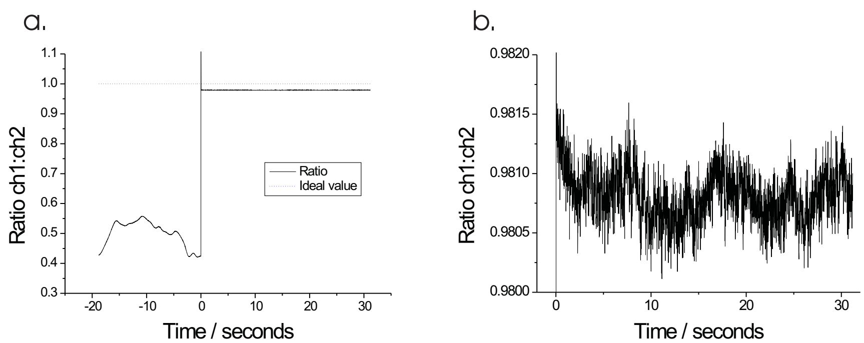

Figure 3.5: Ratio of detector signals using the controller. Control was turned on at $t = 0$. (b) shows the same test as (a), though on a different scale.

The controller has a systematic error of 1.9% from the ideal. Op-amps have trimmable offsets, though in the controller used, this offset was left unconnected in both the differential amplifier and PI-controller, assuming that the offset effect would be small. The differential amplifier functions correctly without the offset (ie $V_o < 1$mV, when V_1=V_2). The PI-controller, however, controls to a non-zero value. This is responsible for the systematic error.
The high frequency noise of amplitude 10^{-3} seen in figure 3.5b is technical noise from the detectors and oscilloscope.
Figure 3.5b also shows drift of amplitude 10^{-3} on a time scale of seconds. This is a factor of ten better than the accuracy requirement of 1% stated in section 1.3.

The maximum value of the entanglement achievable is limited by the degree of squeezing. The value of 1% was given as it would ensure that the error caused by the phase instabilities are significantly lower than the error in the squeezing value, and so the limit set by the squeezing is indeed reached. To make the phase stabilisation significantly better than 1% does not gain anything, due to the error in squeezing. For the current experiment then, the accuracy of the first controller, once the offset has been set, is sufficient.

3.4 Second controller

The first controller was built, as described in section 3.3, using values of R_3, R_4 and C_1 that seemed required for the drift observed. The quality of control that was in principle possible was not known. When the controller was tested, the major drift was suppressed, though there remained smaller drift about the ideal, of amplitude 10^{-3} on a time scale of seconds. While this was sufficient for the present accuracy of the experiment, it was decided to investigate what accuracy of interference phase was in principle possible. This would mean that if and when other causes of error were corrected in the system, the phase stabilisation would have been fully investigated, and not need to be revisited.

To improve the control still further it was decided to carry out a computer simulation of the controller's behaviour, and thus optimise the choice of components used. The circuit layout used was the same as that for the previous controller, shown in figure 3.4.

3.4.1 Characterisation of the system response

When controlling the interferometer, a finite time is required for the control signal to be amplified, the piezo to move, and the detector to register that the light level had changed. This is the response time of the system. To simulate the behaviour of the controller and its effect on the system, the computer required that this response time be measured. It also required the frequency and amplitude of the oscillations that needed to be regulated against. To measure these, the uncontrolled system was perturbed by deliberately changing the voltage sent to the amplifier, as shown in figure 3.6. This simulated, in a very stylised way, the change in voltage that the amplifier would receive from the PI-controller in the case of the controlled system.

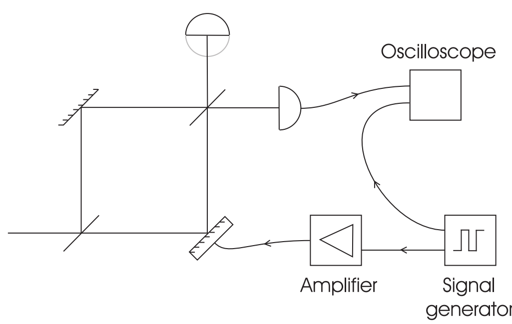

Figure 3.6: A periodic perturbation is given to the piezo, to measure the response time of the system

It was not possible to measure the responses of the individual components; the amplifier output was $\sim$ 500 V, which was too high to measure directly with the oscilloscope, and there was no simple, accurate way to measure the displacement of the piezo. This lack of detail as to the exact working of the interferometer did not detract from the model, as the entire stretch from amplifier to detector could simply be characterised by one number: the rise time.

The signal generator gave a square wave function with amplitude 0.9 V and frequency 0.242 Hz. The exact frequency was unimportant, provided the period of the square wave

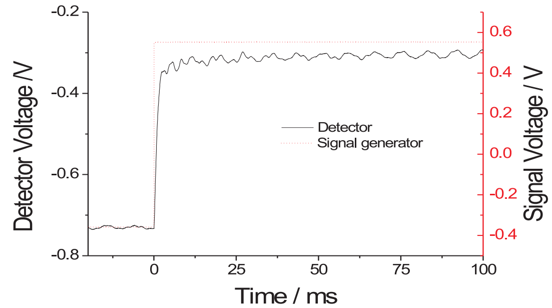

Figure 3.7: Response of the uncontrolled system (as in figure 3.6) to a step perturbation.

was at least twice as long as the system response time. Were this not the case, the signal generator would change to a new voltage before the detector had finished responding to the previous change, and information about the final stabilisation of the system would not be measured. From component data sheets [22, 36] a response time of the order of milliseconds was expected.

The response of the system to this perturbation is shown in figure 3.7. The response time is 1.5 ms. There are initial oscillations of period 3 ms which have decayed within 50 ms of the step, leaving oscillations of 8 ms, which continue undamped. The source of these 8 ms fluctuations was later found to be technical noise from the laser. Under correct operation the laser has a well defined repetition peak at 82 MHz. The laser can however lase in a regime where it runs unstably, giving rise to numerous side bands in the frequency spectrum. These were the source of the oscillations. Such oscillations did not effect the testing in section 3.3.2 as the ratio of the two detector signals, and not the absolute value, was taken. The oscillations do not effect the degree of entanglement as the phase relation remains the same. They are generally not present in entanglement experiments as the laser is always carefully set so that it operates in mode without sidebands, for reasons of good detection of quantum noise at 17MHz.

3.4.2 Simulation

Model interferometer

A computer model of the interferometer was designed using Matlab [37], the layout of which is given in figure 3.8. The interferometer was modeled to have essentially the same response as the physical system.

The amplifier, piezo and detector are shown as three separate boxes in the diagram only so as to see where the apparatus is. As nothing is known about the response of the individual items, the response of all three is put together in one operation. This response is characterised by the 1.5 ms rise time. Following the detector, a sinusoidal perturbation of period 4.5 ms was added. The origin of the perturbation in the experiment was not known at this point. It was assumed to be an oscillation due to the optical path lengths of the interferometer

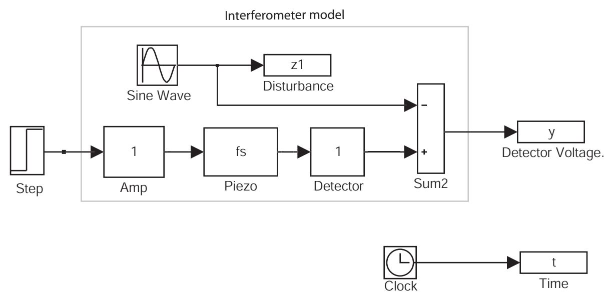

Figure 3.8: Matlab model of the interferometer. As with the experiment, step function is given as a perturbation, and the interferometer takes some finite time (fs) to react. On top of this is added a periodic disturbance.

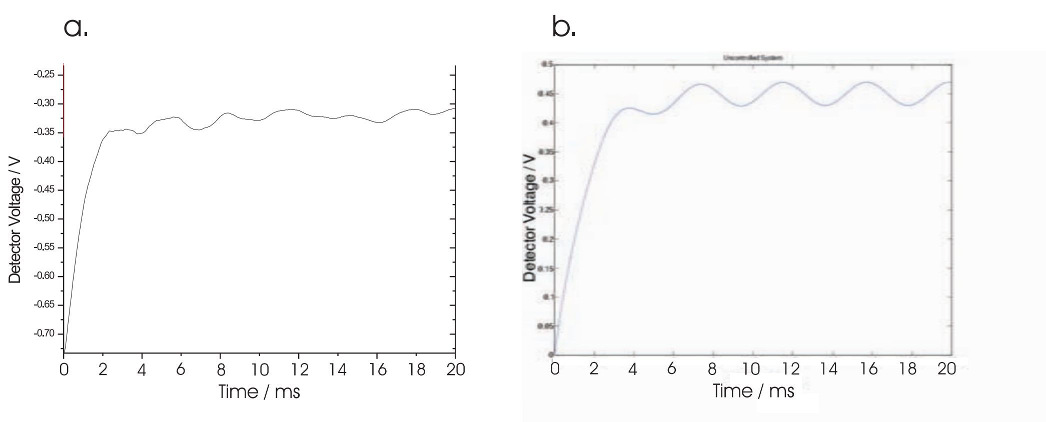

Figure 3.9: (a) shows the actual response of the system to a given perturbation. (b) shows the response of the computer simulation, shown in figure 3.8 to the same perturbation.

changing and was therefore added within the control loop. This meant the oscillations would be suppressed by the simulation. Had they been added outside the loop, then the PI-control would not have regulated against them. In the real system, the oscillations do in fact come from outside the loop. This does not cause problems as they are not usually present in the experiment, and they cause no change in phase. The response of the uncontrolled model interferometer is shown in figure 3.9b.

Model of feedback

The model of the interferometer described above, was put into a system that simulated the reponse of a PI-controller. This is shown in figure 3.10. A step function was given as an input signal to the model PI-controller, and the computer calculated the response of an ideal PI-controller, given user-specified values of K_R and T_N. The real controller had certain limitations which the model did not. The greatest of these was that the model controller gave a signal exactly as predicted by the proportional and integral parts of eq (3.3). The physical

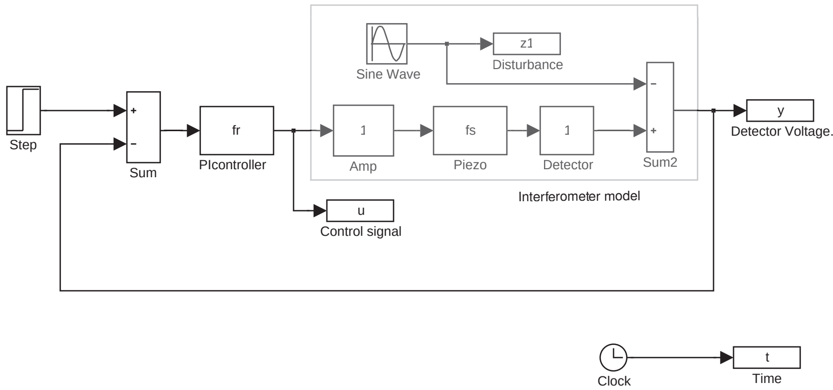

Figure 3.10: The model interferometer in a control loop which simulates the behaviour of a PI.controller.

controller is limited by the maximum output voltage that the op-amp is able to give, which is around 10V. This limit does not severely alter the response that the system gives, except that the initial correction of the physical controller will be a little slower. In practice this should not cause difficulties, as the step function is an artificially sharp perturbation. In normal use the controller will not have to regulate anything so fast, and so the op-amp should not reach its voltage limit. To complete the feedback loop, the response of the interferometer to the PI-controller signal was fed back to the PI-controller.

Choice of parameter values

Given this feedback system, the computer calculated the response to a step function for the stated values of K_R and T_N. These could be varied by the user until a reasonable response was given. The final parameters were thus chosen by an iterative method of trial and improvement. The computer did not optimise the results, nor guarantee that the parameters chosen were the best possible in that situation; it only gave the response for any chosen pair of parameters. The optimisation was left to the judgement of the user. The final parameters chosen were:

$$\begin{aligned} K_R &= 100 \\ T_N &= 0.5\text{s} \end{aligned} \tag{3.5}$$

The following component values were therefore chosen:

$$\begin{aligned} R_3 &< 500\Omega \\ R_4 &< 10\text{k}\Omega \\ C_1 &= 9.4\text{nF} \end{aligned}$$

From the Bode diagram in figure 3.11 it can be seen that the oscillations against which the controller is endeavouring to regulate, notably those of order 1 Hz (0.15 radians per second), should be suppressed by 40dB, ie a factor of 10^4.

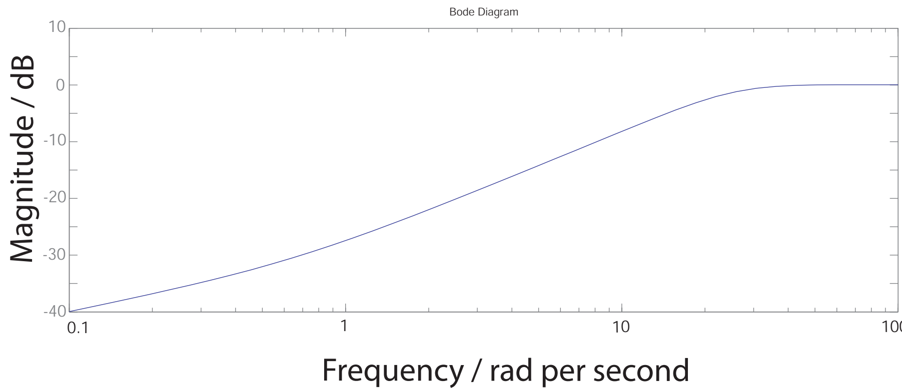

Figure 3.11: Theoretical suppression of the disturbance as a function of frequency for the parameter values in eqs 3.5.

3.4.3 Testing of the controller

Method

• Testing against a step function.

Under normal operation, the two inputs to the controller, V_1 and V_2, are the signals from the two detectors. The controller then moves the piezo until these two values are equal. However, to obtain a direct comparison with the simulation, one of the inputs, V_1, was connected to the signal generator, which gave a square wave of amplitude 0.125V. Ideally, the controller would then move the piezo until the detector output was equal to the signal generator voltage. This should then mean that the detector voltage follows the step function, as was done in the simulation.

This was done initially for the values of R_3 and R_4 that were obtained from the simulation. The values of resistance were then tuned empirically so as to give good control. The results of these tests are shown in figures 3.12 and 3.13.

• Testing the phase regulation

Using the component values obtained in the simulation, the two detector signals were used as inputs, and the controller was set to regulate the phase, as would be done under normal experimental conditions where phase stabilization was required. The results of this are shown in figure 3.14

Results

Using the component values predicted by the simulation, it is clear that under some conditions, the control gives rise to strong oscillations (figure 3.12). The amplitude of the oscillations are dependent the value of R_3; their amplitude increases for smaller resistances. Beyond this, their exact cause is not known. While for a step the control is not stable, under normal operating conditions, the behaviour of the controlled signal is much better.

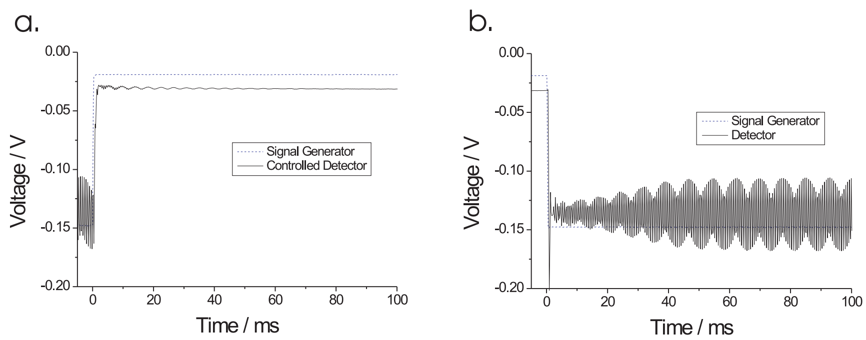

Figure 3.12: Response using values from the simulation. One input to the controller is the detector, while the second is the signal generator. When the signal changed to a less negative voltage (a), the controller responded well. When the step was to a more negative voltage (b) the controlled detector signal oscillated.

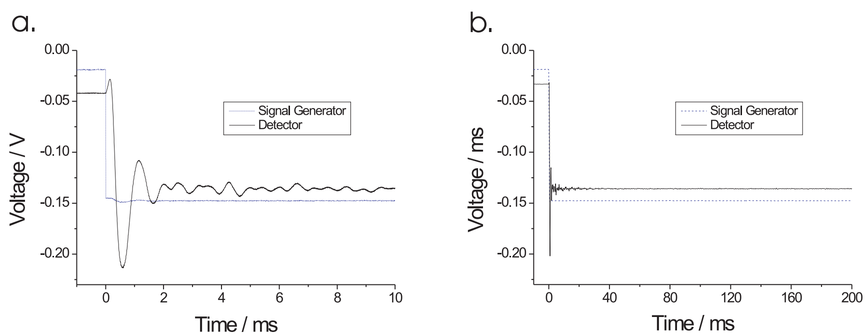

Figure 3.13: Response using values of R_3 and R_4 which were found empirically. Apart from the resistor values the set up was as described for figure 3.12. Initially, the controlled signal oscilates (a), but these oscillations quickly decay, and the value is held constant.

By altering the variable resistors, a good response was obtained for the values:

$$
\begin{aligned}
R_3 &= 230\Omega \\
R_4 &= 5\text{k}\Omega \\
C_1 &= 9.4\text{nF}.
\end{aligned}
$$

These give the parameter values:

$$
\begin{aligned}
K_R &= 21.7 \\
T_N &= 21 \times 10^3\text{s}
\end{aligned}
$$

Once again, the controller has an offset, as the PI-controller is not regulating to exactly zero (see section 3.3.2). The drift has been suppressed to $\sim 3 \times 10^{-4}$. This is equivalent to a change in phase of 1.5×10^{-4}radians. The uncontrolled system has a phase drift of $\frac{\pi}{2}$ radians.

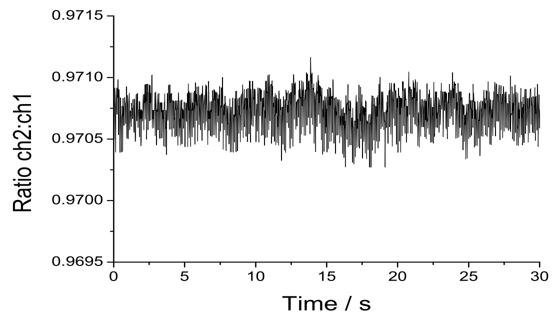

Figure 3.14: Ratio of the two detector signals using the new controller. Values of R_3 and R_4 are those obtained from the simulation.

This agrees well with the prediction from the simulation that the controller should be able to give 40dB suppression.

Without the offsets being corrected, the phase error in the interference phase is much smaller than has in the uncontrolled system, though larger than the aim set initially. Once this has been corrected, the second controller would give an error of better that two parts in ten thousand, which is well below the level of uncertainty in the squeezing, and well within the initial aim of 1%. The simulation showed that this accuracy is the best that can be achieved by the method described, given the response time of the interferometer.

Chapter 4

Conclusions and outlook

4.1 Conclusion

This project aimed to stabilise the source of bright, entangled beams used by ZEMO in Erlangen, so that consistently high entanglement could be achieved. To do this, it aimed firstly to stabilise the long term drift in the power of the laser system, so that a constant degree of squeezing could be obtained. Thereafter it aimed to control the interference phase of the interferometer used to an accuracy better than that of the squeezing, so that the maximum entanglement allowed by the degree of squeezing could be realised.

It was shown that, using the power stabilisation system proposed, and by correct choice of parameters the power can be controlled to within between 0.75 and 0.5% of the set value, where the uncertainty is due to different accuracies at different incident powers. Experimentally the long term drift of the laser system was removed, and the power stabilised to within 0.75% of the set value. This is equivalent to an error of 0.5dB, or 12%, from the optimal squeezing value.

The phase was then stabilised using an electronic feedback scheme. Using a simulation it was shown that a suppression of the drift by a factor of 10^4 was possible. This suppression was experimentally realised, and the final, suppressed drift is equivalent to an error in phase of 1.5×10^{-4}radians. There was also a systematic offset in the regulation of up to 2.2%, depending on the controller used. This error is smaller than the error due to squeezing, and once the offset has been corrected, will be much better than the error due to squeezing.

4.2 Outlook

For the present experiment, the accuracy achieved for laser stabilisation is sufficient. If higher precision were required in future experiments, the largest source of error is the limit set by the step size. This could be reduced by changing the existing 1:5 gearing ratio to a yet higher ratio.

The largest source of error for the controller is the systematic offset. The offset trimmer should be connected in the controller. This can be done using the circuit shown in figure 4.1.

The phase stabilisation is currently being used in the train shown in figure 1.6. However, this method of phase stabilisation involves the detection of the two output beams. This

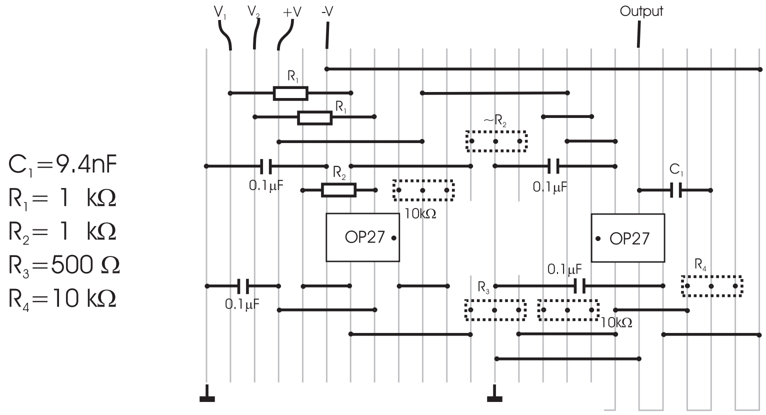

Figure 4.1: Circuit layout for the differential amplifier and controller. The offsets are the two 10kΩ variable resistors.

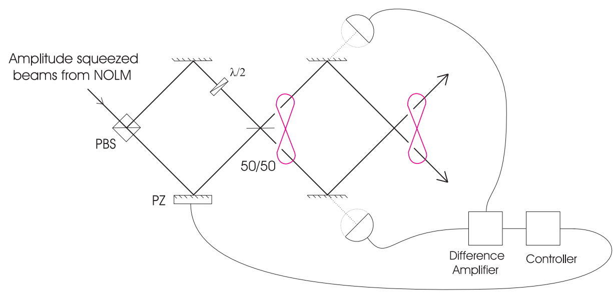

Figure 4.2: Stable entanglement source after which the beams can be used. Up to the 50:50 beam splitter, the train shown here is the same as that in figure 3.1. The phase stabilisation works in the same way as before, but only a small fraction of the beam is monitored, leaving the rest of the beam to be used for further experiments, such as entanglement swapping.

demonstrates entanglement, but the act of measurement destroys the beams. If the beams are to be used for quantum communication, then the present method of stabilisation will not work. Ideally, the beams' intensity should be monitored, while leaving the beams essentially intact, to be used for further applications. This can be achieved by reflecting the entangled beams from gold mirrors. The mirrors are not perfectly reflecting, rather 0.5% of the incident light is transmitted. As the beam intensity is $\sim$ 3.5 mV, a detector capable of measuring accurately a signal of 17 μW could be placed behind a mirror to monitor the signal. It has been shown that the detector described in chapter 2 can be placed behind a mirror and monitor the power accurately enough to be used in a phase stabilisation scheme, leaving the two entangled beams to be used for other applications as shown in figure 4.2. Using this method of phase stabilisation, a train to demonstrate entanglement swapping is being built.

Appendix A

Component List

A.1 Phase stabilisation

Component	**Manufacturer/ Supplier**	**Part/ Order No.**	**Details**
Strip board	RS components	434-116	
Resistor	Conrad Electronics	287-235	1kΩ
Potentiometer	RS Components	154-216	500Ω
Potentiometer	RS Components	154-2038	2kΩ
Potentiometer	RS Components	154-2050	10kΩ
Capacitor	RS Components	405-7741	4.7nF
Capacitor	RS Components	829-615	0.1μF
Diode	RS Components	287-235	BAS16
Op-amp	Analog Devices	411-090	
BNC socket	Electronic workshop		
Co-axial socket	Electronic workshop		
Steel housing	Electronic workshop		44mm$\times$48mm$\times$80mm $\times$80mm

A.2 Laser stabilisation

Component	**Manufacturer/ Supplier**	**Part/ Order No.**	**Details**
AD card	National Instruments	PC-LPM-16PnP Board	
Step motor	Conrad Electronic	967645-22	
motor card	Conrad Electronic	967599-22	
4 pole DIN socket	Electronic workshop		
4 pole DIN socket	Electronic workshop		
Aluminium housing	Electronic workshop		45mm$\times$110mm $\times$220mm
Photo detector	Epitaxx	ETX500T	
Circuit board	Electronic workshop		Cu:Sn rails
Resistor	RS Components	223-2085	47Ω
Capacitor	RS Components	298-9258	100pF
Capacitor	RS Components	264-4337	1nF
Capacitor	RS Components	264-4371	10nF
Capacitor	RS Components	264-4416	100nF
Capacitor	RS Components	264-4214	1μF
Inductor	RS Components	254-7040	1μH
Inductor	RS Components	254-7056	1.5μH
Inductor	RS Components	191-0318	2.2μH
Inductor	RS Components	181-0324	3.3μH
Inductor	RS Components	191-0368	6.8μH
Op-amp	Analog Devices	411-090	
Solder	RS Components	361-1990	Sn:Pb:Cu Single core
BNC socket	Electronic workshop		
5 pole DIN socket	Electronic workshop		
Steel housing	Electronic workshop		33mm$\times$40mm $\times$70mm
Half-wave plate	Linos		1/2” Quartz Optimised - 1530nm
Rubber belt	Contitech	HT D201-311Q	
Polarisation beam splitter	Bernhard Halle Nachfl.	Custom	10mm$\times$10mm $\times$10mm
Mounts	Thor Labs	Various	

Appendix B

Calculations

B.1 Extreme resolution of the step motor

The transmission curve of the half-wave plate is given by:

$$P = P_{inc} cos^2(2\theta) \tag{B.1}$$

where P is the transmitted power,
P_{inc} is the power incident on the half-wave plate

So as to transmit P_{reg}, the wave plate must be at a certain angle, dependent on P_{inc}, namely:

$$\theta' = \frac{1}{2} \cdot cos^{-1} \left(\sqrt{\frac{P_{reg}}{P_{inc}}} \right) \tag{B.2}$$

Where $\theta\prime$ is the value of θ that allows P_{reg} to be transmitted. The gradient at this point is:

$$\begin{aligned} \left.\frac{dP}{d\theta}\right|_{\theta'} &= -4P_{inc} \cdot \cos(2\theta') \cdot \sin(2\theta') \\ &= -4P_{inc} \sqrt{\frac{P_{reg}}{P_{inc}}} \cdot sin \left(2 \cdot \frac{1}{2} cos^{-1} \left[\sqrt{\frac{P_{reg}}{P_{inc}}} \right] \right) \end{aligned} \tag{B.3}$$

In the extreme case where P_{inc}^{max} is incident, and noting that $P_{reg} = 0.85\, P_{inc}^{mid}$ and $P_{inc}^{max} = 1.1\, P_{inc}^{mid}$, eq (B.3) can be simplified to:

$$\begin{aligned} \left.\frac{dP}{d\theta}\right|_{\theta'} &= -4 \times 1.1\, P_{inc}^{mid} \sqrt{\frac{0.85}{1.1}} \cdot sin \left(cos^{-1} \left[\sqrt{\frac{0.85}{1.1}} \right] \right) \\ &= 1.84\, P_{inc}^{mid} \text{ per radian} \end{aligned} \tag{B.4}$$

Given the step size of the motor from eq (2.2), this gives a power resolution per step of:

$$\begin{aligned} R_M(P) &= 1.84 P_{inc}^{mid} \text{per rad} \times 6.5 \text{mrad per step} \\ &= 12 P_{inc}^{mid} \text{ per step} \end{aligned} \tag{B.5}$$

In the same fashion, but inserting the value $P_{inc}^{min} = 0.9\, P_{inc}^{mid}$ into eq (B.3), the resolution in the case of minimum incident power can be calculated to be 5.4 P_{inc}^{mid} per step.

B.2 Differential amplifier component tolerances

The circuit shown in figure 3.2 behaves as:

$$V_o = \frac{V_2 \cdot (R_1 R_4 + R_2 R_4) - V_1 \cdot (R_2 R_3 + R_2 R_4)}{R_1 \cdot (R_3 + R_4)}. \tag{B.6}$$

Assuming that the output signal, V_o is controlled correctly to zero by the PI-controller, the ratio of the two input voltages is given by

$$\frac{V_1}{V_2} = \frac{R_4 \cdot (R_1 + R_2)}{R_2 \cdot (R_3 + R_4)}. \tag{B.7}$$

The absolute values of the resistances do not matter, only their ratios, and so any deviation from the ideal resistances can be characterised by an effective change to the value of only one resistor.

Let R_1, R_2, R_3 and R_4 be some ideal resistances that satisfy the equation:

$$\frac{R_2}{R_1} = \frac{R_4}{R_3} \tag{B.8}$$

(ie eq (3.2)), and then say that in the experiment, resistances of values R_1, R_2, R_3 and $R_4 + \varepsilon$ have been used. In this case, for V_o equal to zero, the ratio between inputs is

$$\frac{V_1}{V_2} = \frac{R_4 \cdot (R_1 + R_2) + \varepsilon \cdot (R_1 + R_2)}{R_2 \cdot (R_3 + R_4) + \varepsilon \cdot R_2} \tag{B.9}$$

The tolerance on each of the four resistances is $\pm$ 1%, giving an effective tolerance, ε, on just one resistor of $\approx$ 4%. Using this value in equation B.9, a systematic error of up to 2% from unity is possible.

This error can reduced by replacing one of the resistors with a variable resistor, and tuning the resistance so that for equal inputs, V_o is zero.

Appendix C

LabVIEW

C.1 Bit values for the eight steps

Bit no. / Step	1	2	3	4	5	6	7	8
a	1	1	1	0	0	1	1	0
b	1	0	1	1	0	1	1	0
c	0	0	1	1	1	0	1	0
d	1	0	1	1	0	0	1	0
e	1	1	0	0	0	0	1	0
f	1	0	0	1	0	0	1	0
g	0	0	0	1	1	1	1	0
h	1	0	0	1	0	1	1	0

C.2 Extracts from the code

C.2.1 Steps

All the *step* programs are the same, with the exception of which control bits they send. Figure C.1 shows *step g* as an example. Figure C.1a. shows the front panel, with which the user interfaces. The Parallel Port Input field is where the bits to be sent are chosen (in this case, the step will sent 00011110). Once they are sent, the sub*vi* confirms this by printing the bits sent in the Parallel Port Output field. The value “37A” and “378” for the strobe address and memory address (bottom left) are the addresses of pin 1 and pin 2 of the printer port, respectively.

The step works in three stages, as shown by figure C.1b, c and d. When the step is called, the “strobe input on” field sends a bit to turn the strobe signal on (b). In figure C.1c, the *step* then sends the contents of the Parallel Port Input field, plus or minus a factor dependent on the motor number, to the memory address specified. In the example given, 64 is subtracted from the input, so as to send the control bits to motor number 1.

Finally, the *step* turns the strobe signal off. As the strobe is active low, this prompts the card to read off the values of the bits that have just been sent.

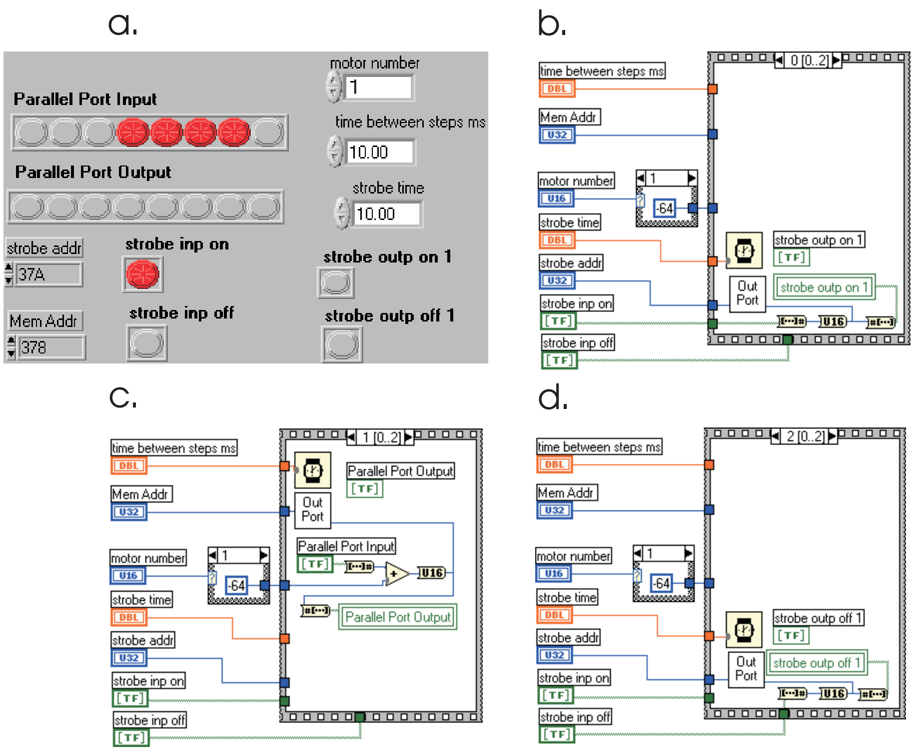

Figure C.1: LabVIEW code for *step g*.

C.2.2 Measurement

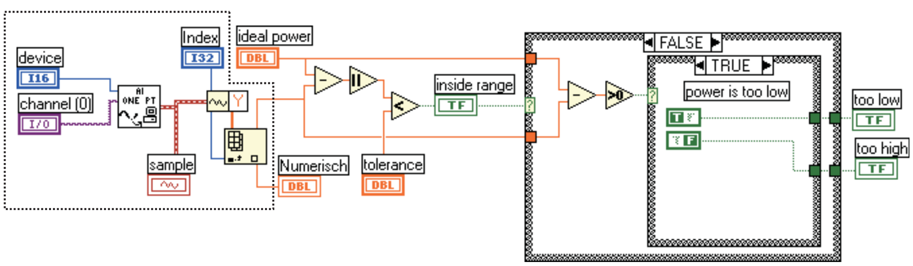

Figure C.2: Typical view of the LabVIEW code for *measurement*.

Figure C.2 shows, a typical portion of the code for *measurement*. Working from left to right, *measurement* takes a detector reading and compares it to the ideal power. The code in the dotted box which takes the detector reading was adapted from a data acquisition program by Stefan Lorenz. *measurement* then takes the difference of the ideal and measured values, and compares this with the tolerance. If the measurement is inside the range, ie the “inside range” has a value of true, then the program pauses, and takes another measurement. If the “inside range” has a value of false, as shown here, then *measurement* works out whether the value is too high or too low, and sets the appropriate truth values for “too low” and “too high”.

C.2.3 Feedback

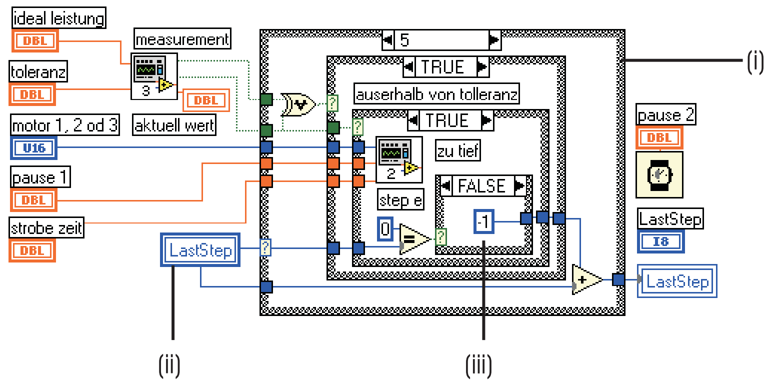

Figure C.3: Typical view of the LabVIEW code for *feedback*.

Figure C.3 shows a typical view of *feedback*. The ideal power and tolerance are entered by the user on the front panel (not shown). *measurement* then works out whether the power is to high or too low (see above). The largest of the boxes (i) is one of eight possibilities, depending on which state was sent last. The “last step” field (ii) chooses from between these eight options. Knowing what the last step was, and in which direction the motor needs to turn, if at all, *feedback* can then call the correct *step*.

The small box labeled iii ensures that the “last step” counts in modulo 8. When turning to increase the power it will subtract one from the last step at each iteration, until the last step is smaller than zero, when it will add 8.

C.2.4 Control

Figure C.4a shows the front panel seen by the user. The motor number, ideal power, and tolerance can be specified, as can the times of various pauses, though these only take effect with continuous rotation. The front panel also shows the current detector signal (“Aktuelle Wert”). Using the toggle switches, the user can chose between regulation (“reglung”) and constant rotation (“drehen”). If the front panel is set to regulate, then *control* calls feedback, and sends it the user specified values from the front panel (b).

If the rotation mode is chosen, feedback is sent the user specified values, as before, but also told that the detector signal is, in this case, -1000V. *feedback* continually rotates in a vain effort to correct this. Even in the rotate mode, the Aktuelle Wert field gives the correct detector signal.

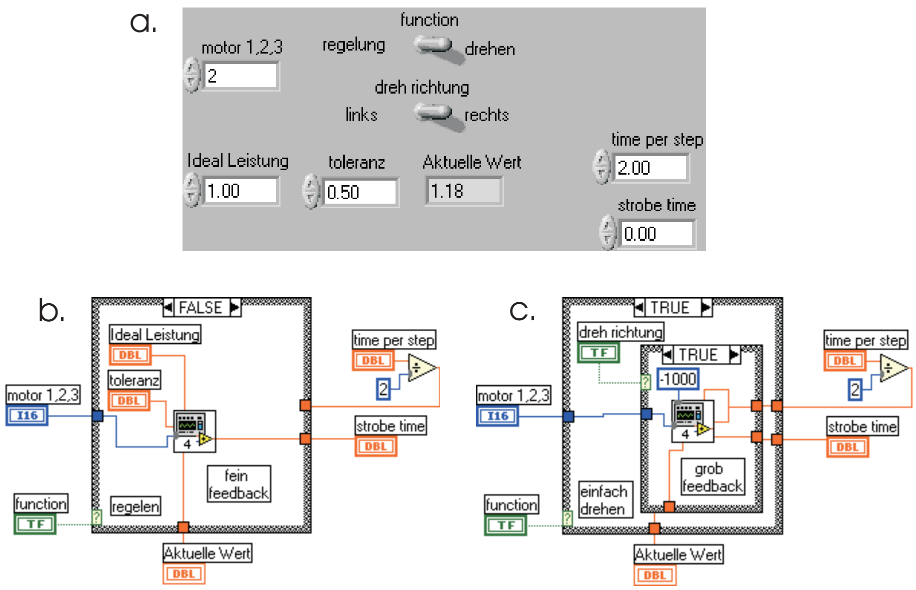

Figure C.4: LabVIEW code for *control*. (a) shows the front panel, while (b) and (c) are the code for regulation and rotation respectively.

Appendix D

Detector Layout

Combined AD/DC design

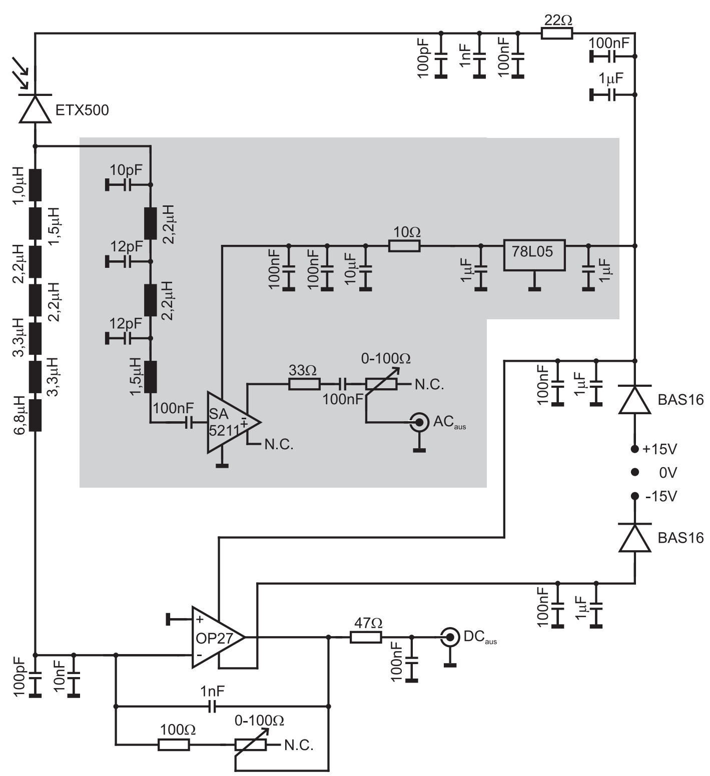

Figure D.1: Combined AD/DC detector circuit.(Adapted from [26])

Figure D.1 shows the circuit used for the combined AD/DC detector which was developed by Michael Langer. The shaded area is for AC detection, and was removed to give the DC detector design.

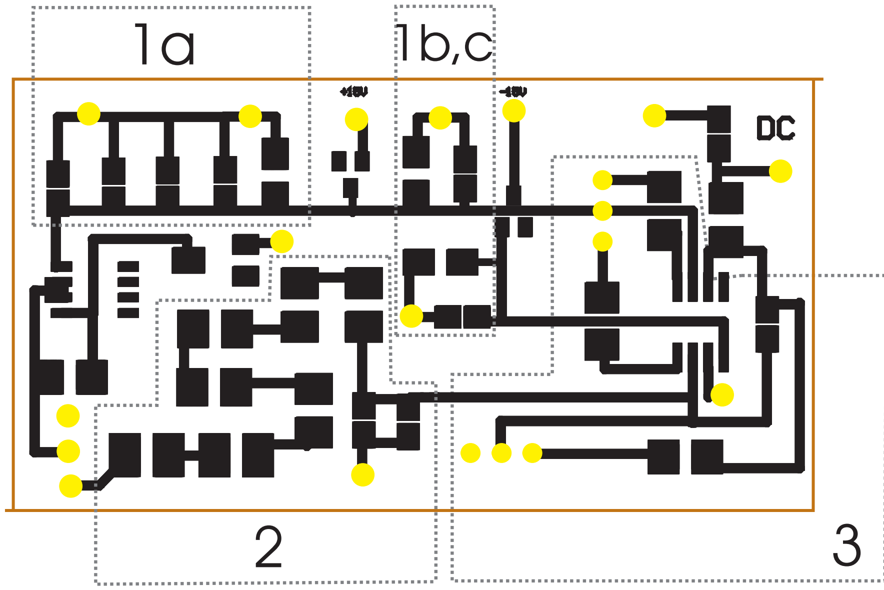

Figure D.2: EAGLE PCB design for the DC detector.

DC detector PCB design

Figure D.2 shows the PCB circuit designed for the circuit shown in figure 2.12. The three circles at the bottom left are the connection to the photo diode. The circle at the top left below the "DC" label is the DC output. The areas in the dotted boxed correspond to the sections shown in figure 2.12.

Bibliography

[1] P. Shor. *Algorithms for Quantum Computation: Discrete Logarithms and Factoring.* IEEE Symposium on the Foundation of Computer Science. (1994)

[2] D. Boumeester, A. Ekert, A. Zeilinger. *The Physics of Quantum Information.* Springer. (2000)

[3] C. Bennett, G. Brassard. *Quantum Cryptography: Public Key Distribution and Coin Tossing.* Procedings of the IEEE International Conference on Computer Systems and Signal Processing, Bangalore, pp175-179. (December 1984)

[4] *QKDS v 1.0 specifications.* idQuantique. (February 2002)

[5] G. Leuchs, T. C. Ralph, Ch. Silberhorn, N. Korolkova. *Scheme for the Generation of Entangled Solitons for Quantum Communication.* Journal of Modern Optics, **46**, 14. (1999)

[6] N. Korolkova, F. König, S. Lorenz, M. Meißner, Ch. Silberhorn, G. Leuchs. *Quantum Properties of Solitons in Optical Fibres for Optical Communication.* The proceedings of the XXII Solvay Conference "Physics of communication" in a special issue of Quantum Computers and Computing.

[7] F. König. *QND Measurement of the Photon Number.* Doktorarbeit, Universität Erlangen-Nürnberg. (2002)

[8] M. Michler. *Quantum Dots Break New Ground.* Physics World, pp27-28. (March 2002)

[9] Ch. Silberhorn, T. Ralph, N. Lütkenhaus, G. Leuchs. *Continuous Variable Quantum Cyptography - beating the 3dB loss limit.* e-print arXiv:quant-ph/0204064v2. (2002)

[10] I. Abraham. *Quantum Solitons.* Physics World, pp21-25. (February 1999)

[11] N. Korolkova, Ch. Silberhorn, O. Glöckl, F. König, G. Leuchs *Quantum Interferometry with Fibre Solitons - A Direct Experimental Test of Non-Separability.* Proceedings of the 8th Rochester Conference on Quantum Optics. In print.

[12] Z. Ou, S. Pereirra, H. Kimble, K. Peng. Phys. Rev. Lett. **68**, 3663. (1992)

[13] G. Leuchs, N. Korolkova. *Entangling Fibre Solitons - Quantum Noise Engineering for Interferometry and Communication.* Optics and Photonics News 2, 64-69. (2002)

[14] G. Leuchs. *Optik Grundkurs IV: Nichtlinear und Integrierte Optik.* Lehrstuhl für Optik, Universität Erlangen-Nürnberg, Winter semester 2001.

[15] M. Kitagawa, Y. Yamamoto. Phys. Rev. A **34**, 3974. (1986)

[16] O. Glöckl, C. Marquard, M. Brownnutt, C. Silberhorn, N. Korolkova, G. Leuchs. *Verschränkte Helle Strahlen und Quanteninterferometrie.* Frühjahrstagung Osnabrück, Verhandlung der Deutschen Physikalischen Gesellschaft, Fachverband Quantenoptik, 2/2002 Q432.3, p139.

[17] H. Kimble, Y. Levin, A. Matsko, K. Thorne, S. Vyatchinin. *Conversion of conventional gravitational wave interferometers into QND interferometers by modifying their input and/or output optics.* e-print areXiv:gr-qc/000826. (2002)

[18] N. Korolkova, Ch. Silberhorn, O. Glöckl, S. Lorenz, Ch. Marquardt, G. Leuchs. *Direct experimental test of non-separability and other quantum techniques using continuous variables of light.* Eur. Phys. J. D **18**, 299-235. (2002)

[19] N. Lütkenhaus. *Quanteninformationstheorie und Kommunication* Seminare. Lehrstuhl für Optik, Universität Erlangen-Nürnberg, Sommer semester 2001.

[20] M. Reid. *Quantum Correlations of Phase in Nondegenerate Parametric Oscillation.* Phys. Rev. Lett. **60**, 2731. (1988)

[21] M. Albach *Elektromagnetische Verträtlichkeit.* Lehrstuhl für Elektromagnetische Felder, Universität Erlangen-Nürnberg. Summer semester 2002.

[22] Large Area InGaAs Photodiode ETX 500T data sheet, Epitaxx.

[23] Corespondence between Universität Erlangen-Nürnberg and Bernhard Halle Nachfl. 20th February 2001.

[24] *DAQ PCLMP16/PnP User manual.* National Instruments. (1996) Appendix A.

[25] TANDON schrittmotor Typ: KP4M2-203 data sheet.

[26] M. Langer. *Quantenmechanische Rauschmessungen.* Zulassungsarbeit, Universität Erlangen-Nürnberg. (2001)

[27] A. Sedra, K. Smith. *Microelectronic Circuits.* Fourth Edition, Oxford University Press. (1998) Chapter 2.

[28] R. H. Kingston. *Detection of Optical and Infrared Radiation.* Springer-Verlag. (1978) Chapter 6.2.

[29] G. Owen, P. Keaton. *Fundamentals of Electronics Vol. 3.* Harper International Edition. (1967) Chapter 2.

[30] Ch. Marquardt. *Experimentelle Charicterisierung der Quantenkorrelationen heller Lichtstrahlen.* Diplomarbeit, Universität Erlangen-Nürnberg. (2002)

[31] P. Horowitz, W. Hill. *The Art of Electronics*. Second Edition, Cambridge University Press. (1989) p185.

[32] J. Trautner, InMik group, Lehrstuhl für Optik, Universität Erlangen-Nürnberg. (Unpublished)

[33] Personal communication with F. Dittrich, Lehrstuhl für Reglungstechnik, Universität Erlangen-Nürnberg.

[34] F. Fröhr, F. Orttenburger *Einführung in die electronische Reglungstechnik*. Siemens. (1970) p101.

[35] U. Tietze, Ch. Schenk. *Halbleiterschaltungstechnik*, Springer-Verlag. (1983) Equation 26.8. To fit with the convention used else where in this report, $A_P = K_R$.

[36] http://piezomechanik.com/hp011220/piezo_catalog_2000/p57.htm (April 2002)

[37] Simulation program written by the Lehrstuhl für Reglungstechnik, Univerität Erlangen-Nürnberg.

Acknowledgements

First and foremost, I would like to thank Prof. Gerd Leuchs, for being so willing for me to work in the optics department at Erlangen. His helpfulness has made this year a great experience.

I am also indebted to Dr. Natalia Korolkova as head of QIV, for organising my project, and always ensuring that things were running according to plan. I am especially thankful for the theoretical background she provided throughout the project, and the many hours she invested during the proofing stage of this report.

I wish to thank Oliver Glöckl as my supervisor, above all for his great patience. He was always willing to help with any difficulties, both conceptual and experimental. During the year he taught me much about experimental quantum optics and project work in general.

Much of the background to the phase regulation work would not have been possible without the time, experience and crash course in control theory so gladly provided by Dr. Franz Dittrich. I am thankful for the help he provided.

Thanks is due to all the members of the ZEMO group with whom I have worked, and who made my year such an enjoyable experience. Particular thanks are due to Michael Langer for his explanation of high frequency electronics and optical detection; to Stefan Lorenz whose help with learning bilingual LabVIEW was invaluable; and to Johannes Trautner who was willing to share his knowledge and experience of electronic control and step motors.

Finally I wish to thank my girlfriend, Jenni Hodgkinson, for the help she provided during the proofing of this report, and for her patience throughout this project.